

**SMOOTH AND HOMOGENEOUS
PEG-FUNCTIONALIZED POLYSILOXANES FOR
PROTEIN REPELLENCY**

TARNUMA TABASSUM
Project Advisor: Professor Wei Chen

A thesis presented to the faculty of Mount Holyoke College in partial fulfillment of the requirements for the degree of Bachelor of Arts with Honors

Department of Chemistry
South Hadley, Massachusetts

May 2015

We would like to thank the National Science Foundation for financial support.

ACKNOWLEDGEMENTS

The completion of this thesis would not have been possible without the mentorship, support, kindness and generosity of many people.

Foremost, I would like to express my sincerest gratitude to Professor Wei Chen for her guidance and patience as my research advisor. I can confidently say that she has contributed towards molding my personal and academic growth throughout my undergraduate years. Her wisdom, passion and belief in me will surely fuel my future endeavors.

I am deeply grateful to my academic advisor and thesis committee member, Professor Darren Hamilton. His infectious zeal towards chemistry that I experienced in my earlier undergraduate years defined my major.

I am immensely thankful to Professor Giuliana Davidoff for being on my thesis committee and whose ardent devotion towards her academic field is what I hope to emulate in the future.

I am truly ingratiated to Professor Himali Jayathilake for her insight and feedback, which oftentimes directed me towards my next steps while conducting research.

I acknowledge my lab mentors, Wanxin Wang and Ye Tian, for being patient and kind to someone who was conducting research for the first time. I thank them for being outstanding individuals, both academically and personally, and I am glad to have been mentored by them.

I thank all my current and past lab mates – Akchheta, Lizzie, Bhanushee, Lien, Yen, Linda, Kelly, Barsha, Kimberley and Venky – for being some of the most strongly driven women of my acquaintance. I have had so much to learn from each of them, both outside and inside of the lab.

I am happy to have found two gems on the first day of my undergraduate study and am really grateful to Nooria and Sangeeta for their consistent support and friendship in the past four years.

I dedicate this thesis to my parents for believing in me, loving me unconditionally and making sure I am where I want to be.

TABLE OF CONTENTS

	Page Number
ACKNOWLEDGEMENTS	i
LIST OF FIGURES AND TABLES	iv
ABSTRACT	1
CHAPTER I. INTRODUCTION	
1.1 Motivation and objective: designing a protein resistive surface.	2
1.2 An introduction to polydimethylsiloxanes: chemical structure, properties and applications.	5
1.3 PEGylation: a method to provide protein resistance.	11
1.4 Reaction of interest: Thiol-ene “click” chemistry.	15
1.5 Fabricating a smooth and homogeneous platform.	19
1.6 Surface characterization techniques	21
CHAPTER II. EXPERIMENTAL	
2.1 Materials and Apparati	27
2.2 Methods	28
2.3 Surface characterization	30
CHAPTER III. RESULTS AND DISCUSSION	
3.1 Fabricating a PMMS grafted platform for subsequent PEGylation	32

3.2 Fabricating a smoothened SMS 992 substrate	41
PEGylation	
3.3 Effectiveness of PEGylated SMS 992 as protein repelling surfaces	55
CHAPTER IV.CONCLUSIONS AND FUTURE WORK	66
REFERENCES	69
APPENDICES	74

LIST OF FIGURES AND TABLES

	Page Number
Figure 1. Simplified formation of a thrombus due to protein adsorption.	3
Figure 2. The molecular structure of PDMS depicting the flexibility of the Si-O-Si bonds.	6
Figure 3. The role of PDMS in microfluidics.	8
Figure 4. The structure of PMMS.	9
Figure 5. The mechanism of grafting thiol-functionalized PDMS onto silicon surfaces facilitated by surface water.	10
Figure 6. Comparisons P19 EC cell adhesion on glass, bare PEG films and PEG nanostructure modified surfaces in the presence and absence of collagen	12
Figure 7. Scheme depicting the model suggested by Jeon et al adapted by Banerjee et al.	13
Figure 8. The suggested mechanism of protein adsorption relating to release of counter ions and water molecules.	14
Figure 9. The structure of the PEG derivative used in this study.	15
Figure 10. A generic hydrothiolation reaction with anti-Markovnikov orientation.	16
Figure 11. Thiol-ene “click” chemistry between PMMS and EG/OEG.	17
Figure 12. Scheme depicting a generic thiol-ene mechanism.	18

Figure 13. SEM images showing high fidelity between the hard master and the soft stamp cast.	19
Figure 14. The structures of the two reducing agents, DTB and DTT in addition to mechanism of reduction of disulfide bonds by DTT.	21
Figure 15. Cases of the extent of wettability of the surface as shown by the values of the contact angle.	23
Figure 16. Scheme depicting the components of the topography detecting system of an AFM.	24
Figure 17. Preparation of PMMS and subsequent PEGylated substrates.	33
Figure 18. AFM images of SMS 042 and SMS 992 samples.	34
Figure 19. AFM images showing the varied topographies of SMS 992.	35
Figure 20. A comparison between the thickness of the (O)EG layers on SMS 042 and SMS 992.	37
Figure 21. A comparison between the contact angles of SMS 042 and SMS 992 upon the grafting of PEG layers.	39
Figure 22. AFM images of SMS 992 grafted with (O)EG.	40
Figure 23. A comparison between the RMS values obtained from AFM imaging of SMS 992 and SMS 992 grafted with (O)EG.	40
Figure 24. Changes in the SMS 992 layer thicknesses upon addition of increasing amounts of reducing agents, DTB and DTT.	42
Figure 25. Constant contact angles of the SMS 992 layers upon addition of increasing amounts of reducing agents, DTB and DTT.	44

Figure 26. AFM images of SMS 992 layers comparing the resulting smoothness upon addition of varying amounts of DTB and DTT.	45
Figure 27. Changes in the RMS values of the SMS 992 layers upon addition of increasing amounts of reducing agents DTB and DTT.	47
Figure 28. The approximate length of the molecular chain of EG.	50
Figure 29. Comparisons of (O)EG layer thicknesses with and without the use of DTT as a reducing agent in the grafting of SMS 992.	51
Figure 30. Comparisons of contact angles of (O)EG layers with and without use of DTT as a reducing agent in the grafting of SMS 992.	52
Figure 31. AFM images depicting that the addition of DTT to SMS 992 results in different topographies for the (O)EG layers.	54
Figure 32. Comparisons of AFM RMS values of (O)EG layers with and without use of DTT as a reducing agent in the grafting of SMS 992.	55
Figure 33. Preparation for protein adsorption studies.	56
Figure 34. Comparisons of SMS 992 and PEGylated SMS 992 thicknesses before and after adsorption of PBS, albumin and lysozyme.	58
Figure 35. Structures of albumin and lysozyme.	59
Figure 36. Electronegativity differences in the C-S-H bonds on the SMS 992 surface.	60
Figure 37. Comparisons of dynamic contact angles of SMS 992 and PEGylated SMS 992 before and after adsorption of PBS, albumin and lysozyme.	61

Figure 38. AFM images comparing the surface topographies of SMS 992 and PEGylated SMS 992 upon adsorption of PBS, albumin and lysozyme.	63
Figure 39. Comparisons of the AFM RMS values of SMS 992 and PEGylated SMS 992 before and after adsorption of PBS, albumin and lysozyme.	64
Table 1. Comparisons between SMS 042 and SMS 992 grafted silicon wafers in terms of contact angle, thickness and AFM RMS values	35
Appendix 1: PEGylation of PMMS substrates	74
Appendix 2: Calculation of amount of reducing agent in SMS 992 solution	74
Appendix 3: Effect of reducing agents on SMS 992 layers	75
Appendix 4: PEGylation of SMS 992 reduced with 6.0 wt % of DTT	76
Appendix 5: Protein resistance of PEGylated substrates	77
Appendix 6: Calculation of approximate length of OEG chain	78

ABSTRACT

Polydimethylsiloxanes (PDMS) are important organosilicone compounds that offer a wide range of biological and biomedical applications due to their unique structural properties. However, their inherently hydrophobic surface renders them incompatible with biological systems. Hydrophobic surfaces typically adsorb proteins, which leads to undesirable consequences such as biofilm formation and consequent microbial contamination.

The goal of this study was to create a biocompatible platform by modifying the surfaces of PDMS based substrates. Thiol-functionalized substrates were fabricated by reacting silicon wafers with thiol-functionalized PDMS. Unfortunately, the thiol layers as prepared were rough and non-uniform due to disulfide bond formation between reagent molecules. Reducing agents, such as dithiothreitol, applied during the modification reaction, were necessary to generate smooth and uniform thiol layers. The thiol-functionalized substrates were subsequently evaluated as platforms for conjugations of molecules of biological interest. Vinyl-terminated poly(ethylene glycol) of varying molecular weights were “clicked” to the substrates via thiol-ene photochemistry to hydrophilize the surfaces and hence minimize non-specific protein adsorption. The substrates were characterized using ellipsometry, contact angle goniometry, and atomic force microscopy before and after each reaction.

I. INTRODUCTION

1.1 Motivation and objective: designing a protein resistive surface

The search for protein resistive or non-fouling surfaces is prevalent in many fields such as medicine, pharmaceutical sciences, biotechnology, cell biology, analytical sciences, biophysics and food processing since materials interact with the surrounding environment.¹⁻³ More than a decade ago, Nakanishi¹ described the adsorption of proteins onto solid surfaces as “a common but very complicated phenomenon” and this still holds true despite the wealth of research being directed towards the characterization of interactions between proteins and surfaces of materials.

Proteins have the inherent tendency of accumulating on interfaces non-specifically leading to many instances of undesirable events. For example, biomedical implants in contact with the bloodstream have been shown to cause thrombosis.^{3,4} Figure 1 depicts this phenomenon in a simplified fashion. Adsorption occurs onto a material, such as an artificial blood vessel, giving rise to a series of intricate events. Platelets adhere to the interface, triggering the release of the protein thrombin. This forms a fibrin matrix which stabilizes the adsorbed cells and can consequently form aggregates or a thrombus resulting in vascular obstruction at the point of formation. In severe cases,

occurrence of the process in a blood vessel may result in the removal of the thrombus from the surface and consequently, blockage of an artery due to the clot formed.³

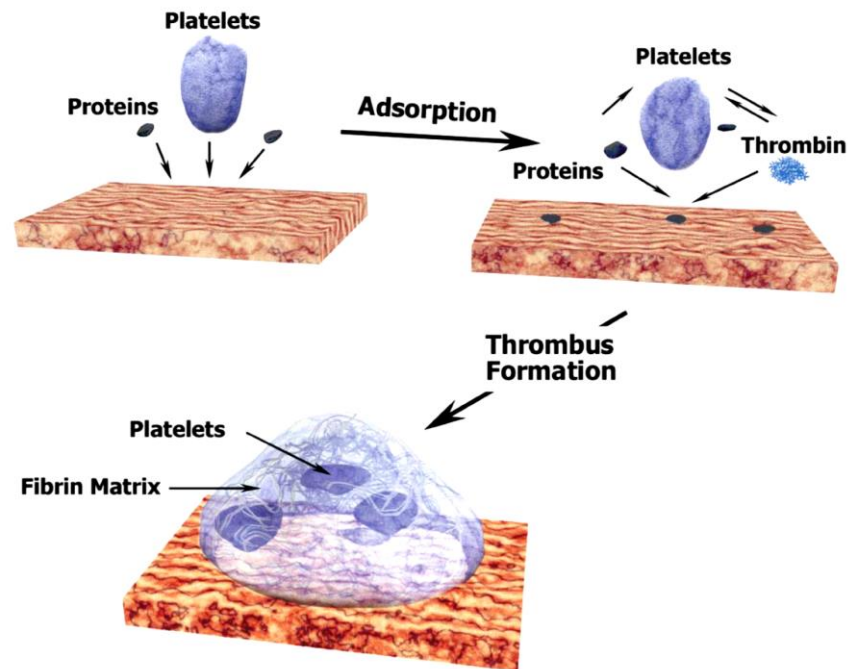


Figure 1. Simplified formation of a thrombus due to protein adsorption.³

Protein adsorption can initiate bacteria, cell or particle adhesion onto surfaces resulting in inflammation cascades, which form scar tissues around the material, or biofilm production leading to microbial contamination.^{2, 3, 5, 6} Its effects are also seen in analytical sciences, where there is degradation of the performance of devices consisting of protein chips, sensor surfaces and assay platforms.²

A methodology of minimizing such protein-surface interactions is to delve into deeper understanding of the seemingly complicated behavior of proteins.

This can be done by answering questions such as why and how do proteins adsorb, which mechanistic rules apply to protein adsorption phenomena or does the adsorption event influence biological functions of proteins. As such, numerous mathematical concepts, model descriptions and computational strategies have been developed to elucidate the event.² Seeking to hinder protein adsorption altogether by use of a material with a protein-resistant surface is a popular choice among scientific communities. That the strength and type of interactions between a material and surrounding proteins are dependent on the interfacial properties of the material is invaluable knowledge and with the goal of minimizing such interactions, prime candidates for such studies are polymer hydrogel modified surfaces or polymer brushes, such as poly(ethylene glycol).³

Adsorption of proteins occurs if the change in total free energy upon adsorption is negative. Adsorption is typically reported to be endothermic suggesting the fact that entropy must be the driving force for adsorption. This can be ascribed to hydrophobic dehydration, that is the release of water molecules, or formation of counter ions or structural changes of the protein.⁶⁻⁹ Typically, protein-resistant surfaces have characteristics such as hydrophilicity, electrical neutrality, and the ability to form a hydrogen bond with water.¹⁰

While non-specific protein adsorption is typically undesirable, efforts are also being directed towards achieving that of the specific type. This kind of

protein adsorption is seen in many natural processes. A current research focus is emulating nature by fabricating materials and assembling them via a bottom-up approach with a hierarchy in the levels of organization so as to exhibit useful biological functions.¹¹

This project, in particular, investigates the grafting of a derivative of the extensively used polymer brush, poly(ethylene glycol), onto polydimethylsiloxane based substrates, a popular biomaterial of choice, so as to create a smooth and homogeneous platform that is immune to non-specific adsorption of proteins. For fabrication of such a protein resistant surface we took advantage of a well-known reaction mechanism, thiol-ene “click” chemistry. To the best of our knowledge, such a model has not been explored before. In order to validate the efficacy of this system, we tested two commonly found proteins, albumin and lysozyme.

1.2 An introduction to polydimethylsiloxanes: chemical structure, properties and applications

Historically important silicone based materials have been used extensively spanning a wide range of applications for the past several decades.¹² Of them, the most common organosilicone is polydimethylsiloxane (PDMS) where alternating silicon and oxygen atoms are bonded to one another, forming the backbone of the polymer chain, and two methyl groups are also attached to the silicon as shown in Figure 2.¹³ Compared to a similar carbon-based backbone

polymer such as polyisobutene, the methyl groups on the silicon atoms and the methyl pairs of PDMS are separated to a greater degree. This is a consequence of the longer Si-O and Si-C bonds (1.63 Å and 1.90 Å) than the C-C (1.53 Å) bond coupled with the wider Si-O-Si bond angle (143°) in comparison with the C-C-C bond angles (109°). There is also less directionality of the Si-O bonds, due to the electronegativity difference resulting in the partially ionic nature of the bonds. Hence, these characteristics of PDMS give rise to vibrational and rotational degrees of freedom not seen in carbon based polymers.¹⁴

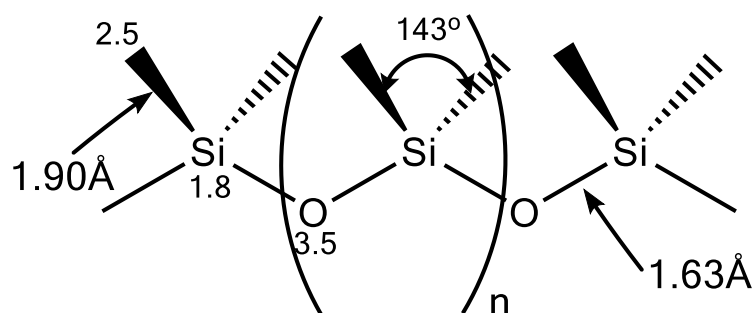


Figure 2. The molecular structure of PDMS depicting the flexibility of the Si-O-Si bonds.¹⁴

As a consequence, PDMS at room temperature is a viscous liquid ($T_g = -125$ °C) with low surface tension.¹⁵ It is inherently hydrophobic with advancing and receding water contact angles as high as $\sim 106^\circ / \sim 105^\circ$, however it is highly permeable to water.^{15, 16} Another dissimilarity between silicones and carbon-based polymers is in the greater thermal stability displayed by silicones. This is attributed to a larger bond dissociation energy

of Si-O and the generation of a solid product, SiO₂, when oxidized in air in the case of silicones.^{14,15} In addition, PDMS is able to achieve optical detection between 240-1100 nm, its electrical properties allow embedded circuits with the capability of intentional breakdown to open connections, it is chemically inert but its surface can be etched or modified and it is also non-toxic.^{17,18} Because of its unique properties, PDMS is a lucrative material for a wide range of applications. These include, but are not limited to, use of PDMS in ophthalmic and blood contacting biomaterials, drug delivery systems, and medical devices such as voice prostheses, catheters and vascular grafts.^{19,20} PDMS has emerged as a key player in biomedical or biological microelectro-mechanical systems (BioMEMS), a prime research area in biomedicine. BioMEMS refers to devices and systems including all interfaces of the biomedical and life science disciplines at the micro- and nano-scale. Directions of research and applications in BioMEMS span from diagnostics to microfluidics, tissue engineering and surface modification, to name a few.^{17,18,21} These devices offer advantages such as reductions of the size of operating systems, use of reagents, production of bi-products and waste, and power requirements as well as a greater flexibility for design, portability, and rapid analysis.²² In the area of microfluidics in particular, the properties of PDMS offer advantages over the traditionally used silicon and glass systems in terms of cost-effectiveness, simplicity in production, ability of conforming to other materials, ability to withstand high temperatures, non-toxicity and

compatibility with optical detection methods. Because of its elastomeric properties, components such as pressure valves, pumps, and channels that allow the execution and automation of the chemical and biological processes can be easily incorporated on the chip.^{17, 22, 23}

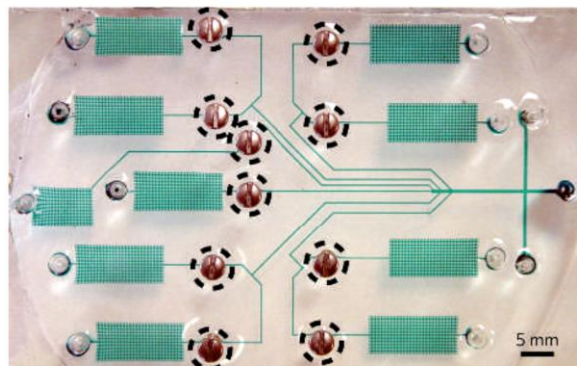


Figure 3. The role of PDMS in microfluidics. The image shows a simple inexpensive microfluidic diagnostic device that performs sandwich immunoassays – tests used widely in medical and biological research.²³

Evidently, PDMS plays a significant role in biomaterials. However, its compatibility is compromised because of its molecular structure. PDMS consists of an inherently hydrophobic surface due to the presence of methyl groups that can contribute to non-specific protein adsorption that can lead to undesirable consequences as discussed in Section 1.1.¹⁴⁻¹⁶ Accordingly, a number of efforts are being directed toward the hydrophilization of PDMS surfaces. These include techniques that physically and/or chemically treat the surface. Plasma oxidation is a popular choice because of its simplicity.^{19, 24} However, plasma oxidation has been shown to provide only a temporary state of hydrophilization to PDMS surfaces as the native hydrophobic state is

quickly recovered, hence more efforts are being focused towards increasing the longevity of the desirable hydrophilic surface.^{19, 24, 25}

Some factors that have been attributed to this recovery are diffusion and migration of low molecular weight (LMW) species of the PDMS from the bulk to the surface, reorientation of polar and non-polar groups between bulk and surface phases, and condensation of the hydroxyl groups on the surface formed due to plasma oxidation.²⁶

Another commonly used surface modification technique is the grafting of polymers onto PDMS based substrates. Polymers that have been explored for this purpose due to their antifouling properties include polyacrylates, oligosaccharides and poly(ethylene glycol) (PEG), the latter being the most extensively used.^{27,28} In this study, we explored the grafting of a PEG derivative onto a thiol-functionalized PDMS based substrate (PMMS) (Figure 4). Two particular compounds, SMS 042 and SMS 992, were initially used as the compounds for experimentation with varying molar concentrations of thiols (5% and 100% respectively).

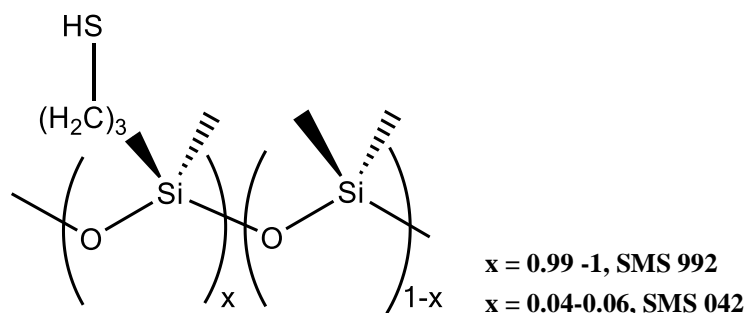


Figure 4. The structure of PMMS is shown. The concentration of –SH groups can vary.

1.3 PEGylation: a method to provide protein resistance

Over the course of the last few decades, poly(ethylene glycol) (PEG) has emerged as an active player in the scientific world. Its journey first began in the late 1960s, when Davis²⁹ of Rutgers University termed it as “the ideal hydrophilic polymer” and looked at its abilities to extend blood life and control immunogenicity of the proteins attached to it. Since then, a plethora of research has been conducted on this polymer that has established its antifouling properties.^{9, 20, 30-33} PEGylation refers to the attachment of oligomeric or polymeric ethylene glycol to surfaces in order to enhance biocompatibility.⁹ Some of the techniques that have been used for attachment of PEG onto surfaces include physical and chemical adsorption, block or graft polymerization and direct covalent attachment.³³ Figure 6 shows an instance of the control of adsorption that can be achieved by altering the structures of the grafted PEG on the nanoscale. It was observed that proteins and cells preferred adhesion to the PEG nanostructures compared with the unpatterned films and, as expected, this extent of adhesion was significantly lower than that of the glass controls.³²

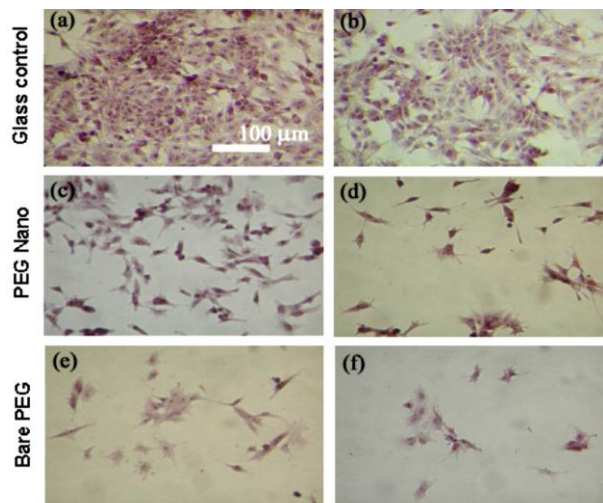


Figure 6. Comparisons P19 EC cell adhesion on glass, bare PEG films and PEG nanostructure modified surfaces in the presence ((a), (b), (c)) and absence of collagen ((d), (e), (f)).³²

Several models have been suggested to explain this protein repelling behavior of PEG. The earliest studies were conducted by Jeon et al. who considered that the PEG chains were terminally attached to a hydrophobic substrate.³⁴ They visualized the protein as a block of infinite length parallel to the substrate with the polymer chains and water in between (Figure 7). When the protein approaches the substrate, the PEG chains are compressed resulting in elastic forces that are repulsive in nature. Furthermore, the presence of a hydration layer prevents close contact of the proteins with the surface. These stresses create repulsive forces where the magnitude depends on factors such as chain length and density of the PEG. They further extended this concept by modeling proteins as finite spheres, concluding that chain length and protein resistance are proportional to one another for a given surface density.³⁵

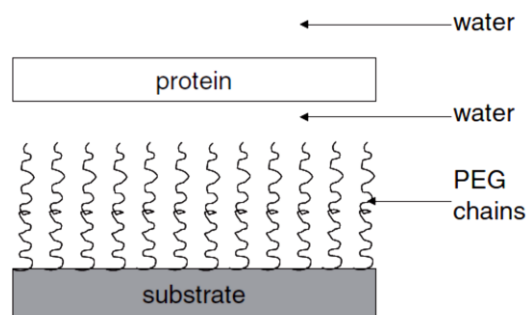


Figure 7. Scheme depicting the model suggested by Jeon et al.³⁴ adapted by Banerjee et al.³³

This model was challenged by other groups and an alternative explanation was attributed to PEG's nature: that the all-trans conformation of the oligomeric ethylene glycol on the surface caused water molecules to be loosely bound to the polymer and were hence easily displaced by the approaching protein molecules compared to the helical conformation which formed a strong hydration layer.³⁶ A more recent model suggests that adsorption does not occur due to absence of counter ion and water release. As a protein molecule approaches an electrically charged surface, counter ions and water molecules are released which result in the entropic gain of the system and subsequent attachment of the protein onto the surface. As discussed in Section 1.1, protein adsorption is an entropically driven process. In the case of the neutrally charged surface of PEG, there is no release of counter ions and water molecules and hence no protein adsorption occurs (Figure 8).⁹

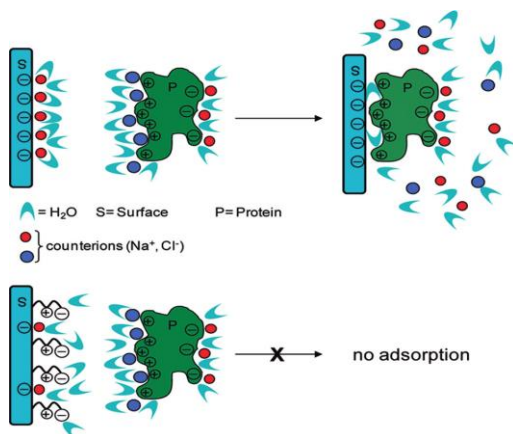


Figure 8. The cartoon depicts the suggested mechanism of protein adsorption relating to release of counter ions and water molecules, which is dependent on whether the surface is charged (top) or is neutral (bottom).⁹

Even though the exact mechanism by which PEG is able to repel proteins is a contested area, the fact that it is able to do so remains irrefutable. In this work, we have taken advantage of this characteristic of PEG so as to modify, or more specifically, hydrophilize the surface of PMMS. To achieve this, we have used a monomeric form of PEG, allyloxy ethylene glycol (EG), as well as a ten-unit form, allyloxy oligo(ethylene glycol) (OEG) (Figure 9) and attached that onto the PMMS substrates discussed in Section 1.2 via the use of a popular reaction mechanism, thiol-ene “click” chemistry. Strictly speaking, the designation of the terms “PEG” and “PEGylation” refer to polymers with much longer chains. However, for the purposes of clarity in this study, we will be using the generic terms PEG and PEGylation to refer to our compounds of interest, EG and OEG.



Figure 9. The structure of the PEG derivative used in this study. $n = 1$ refers to the monomer (EG) while $n = 10$ would depict the structure of the oligomer (OEG).

1.4 Reaction of interest: thiol-ene “click” chemistry

“Click” reactions are relatively a new concept introduced by Sharpless et al in 2001.³⁷ Reactions classified under this category have characteristics such as formation of high yields of desirable products, negligible or minimal by-products that can be easily removed by non-chromatographic techniques, resistance to inhibition by oxygen or water, mild reaction conditions, regio- and stereo-specificity, orthogonality with other synthetic reactions as well as the capability of being accomplished using readily available starting compounds and reagents.³⁷ Particularly, copper-catalyzed azide/alkyne click reactions have achieved widespread fame with a diverse range of applications demonstrating the utility, simplicity and the overall efficient nature of click reactions.³⁸

The use of thiol-ene reactions dates back to 1905 and refers to the hydrothiolation of a C=C bond (Figure 10). It is a mechanism that has been employed in many studies so as to form ideal networks of polymers. Importantly, it has characteristics that categorize it under “click” reactions. A diverse range of enes and any thiol can be employed as substrates although reactivity may differ from one substrate to another.^{38, 39} Thiol-ene reactions

produce significant yields maintaining regioselectivity while requiring small amounts of benign catalysts. The reactions are also rapid, occur in bulk or in environmentally benign solvents and, very importantly, remain unaffected by the presence of oxygen or water. As such, the versatility of thiol-ene reactions makes them the candidate of choice for applications in producing high performance protective uniform polymer networks as well as in processes pertaining to fields such as optics, biomedicine, bioorganic modification as well as sensors.³⁸

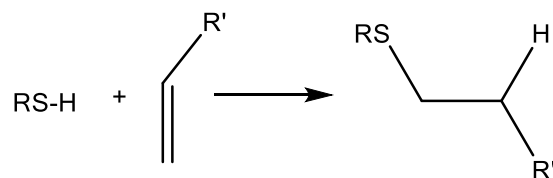


Figure 10. A generic hydrothiolation reaction with anti-Markovnikov orientation.³⁹

In this study, we use a radical mediated thiol-ene process which occurs between a non-sterically hindered terminal, electron-rich, ene or vinyl group (EG and OEG) and a thiol group on PMMS (Figure 11). The resulting network formed from the process is highly homogeneous and has low polymerization shrinkage stress coupled with narrow glass transition regions.^{38, 40} Such characteristics of thiol-ene reactions place them at an advantage over traditional radical based photo polymerization processes involving acrylates and methacrylates.³⁸ Light mediated thiol-ene reactions proceeding via a radical-based mechanism provide the distinctive features of

click reactions with the benefits of simple photo-initiated reactions yielding materials that are tailorable and robust.^{40, 41}

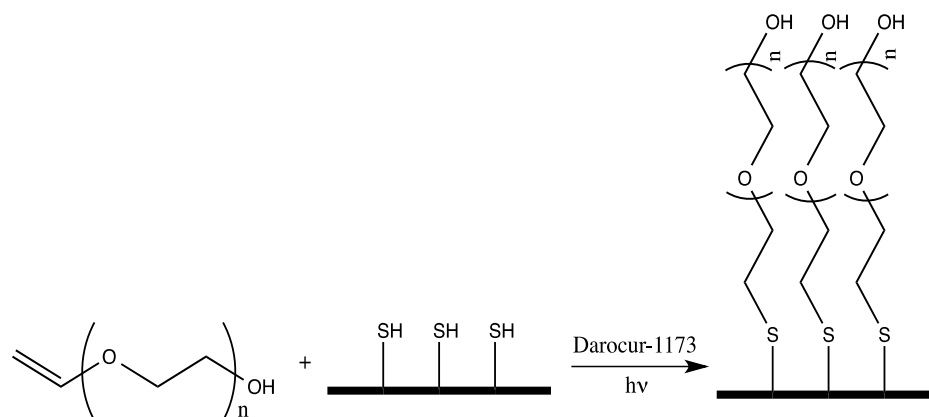


Figure 11. Thiol-ene “click” chemistry between PMMS and EG/OEG. Darocur-1173 was used as the photoinitiator.

Thiol-ene photopolymerization processes follow a radical step-growth polymerization mechanism (Figure 12). The treatment of a thiol with a photoinitiator under irradiation begins the process where, upon abstraction of the hydrogen atom from the S-H bond, a thiyl radical is generated. This is followed by propagation where the thiyl radical is directly added to the electron rich C=C bond which forms a carbon-centered radical which in turn attacks another thiol group, via a chain transfer mechanism, to give an addition product with anti-Markovnikov orientation. A thiyl radical is regenerated, hence restarting the process. Successive propagation and chain transfer mechanisms are the basis for step-growth thiol-ene polymerizations. The reaction is not terminated until all the thiol groups have been incorporated

into the network. As a result, a homogenous system is generated and reaction rates are quite high.³⁹

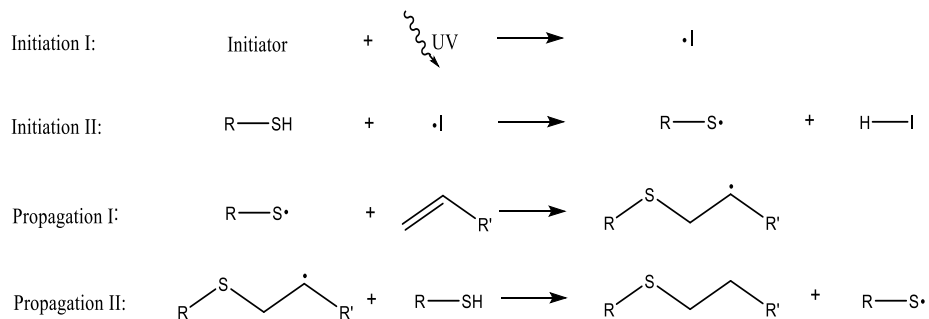


Figure 12. Scheme depicting a generic thiol-ene mechanism. Adapted and modified from a paper by Campos et al, 2008.⁴¹

An instance of the remarkable nature of thiol-ene reactions was demonstrated in a study by Campos et al.⁴¹ By altering the ratios between the thiol-based and alkene-based substrates (incidentally, PMMS and PEG derivatives), they were able to create cross-linked materials for soft imprint lithography at the nanoscale with tunable mechanical properties and robustness. They reported high fidelity between the hard masters and the cross-linked materials suggesting the overall efficiency of such reactions (Figure 13).

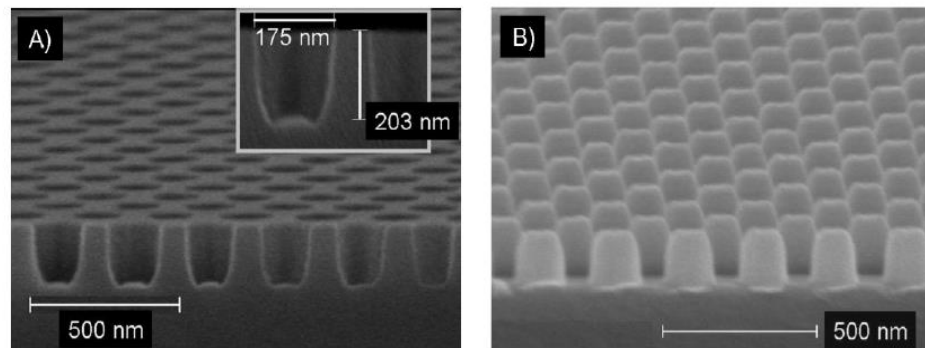


Figure 13. SEM images showing high fidelity between the hard master and the soft stamp cast.⁴¹

1.5 Fabricating a smooth and homogeneous platform

Using PEGylation as a means to modify the surfaces of PDMS based substrates in order to achieve hydrophilization is not an uncommon strategy to reduce protein adsorption. For instance, Sharma et al²⁵ permanently altered the surface of plasma treated commercially available PDMS (Sylgard-184) by grafting with PEG silane rendering it more hydrophilic for use in microfluidic applications, where the fluid velocity in the microchannels of the PEG grafted PDMS increased by four times compared to untreated PDMS. Zhang et al⁴² developed an “environmentally friendly” strategy by modifying surfaces of PDMS microchips by grafting of PEG-NH₂ as a means to drastically improve electrophoretic performances of the microchips to separate proteins as adsorption was prevented whilst ensuring long term stability of the surface. In another study, Sui et al⁴³ described an approach where they oxidized the PDMS surface first by reaction with acidic H₂O₂ in solution phase, followed

by grafting of a PEG derivative so as to successfully fabricate surfaces for passivation of non-specific protein adsorption.

Our approach was to fabricate a substrate consisting of PMMS as the PDMS based substrate and covalently attach EG or OEG as the PEG derivatives via thiol-ene chemistry. Upon initial experimentation with the two compounds, we observed the formation of aggregates on the PEGylated surfaces, as represented by bright spots in atomic force microscopy images. We hypothesized that this was the result of intermolecular and intramolecular polymerization between the thiol groups in the PMMS layers to form disulfide linkages. This issue was addressed in order to provide a uniform thiol-functionalized surface for PEGylation to occur.

Cleland⁴⁴ realized that for an intramolecular reaction, a 1,4-butanedithiol (DTB) (Figure 14 (a)) based structure such as dithiothreitol (DTT) (Figure 14 (b)) would be able to form a sterically favorable cyclic disulfide (Figure 14 (c)) and could be used as a reducing agent to effectively reduce disulfide linkages, keeping the individual thiol groups in the reduced state. Cleland⁴⁴ concluded that this characteristic of DTT as an effective reducing agent was attributable to its very low redox potential at neutral conditions i.e. -0.33 V. DTT has other suitable characteristics such as the fact that both oxidized and reduced forms are water and alcohol soluble, the water solutions being conveniently stable to oxidation in air. In another study, it was concluded that disulfide bonds, which have a relatively low bond energy of ~55 kcal/mol are

reductively cleaved under the presence of reducing agents such as dithiothreitol (DTT) to form thiol groups.⁴⁵

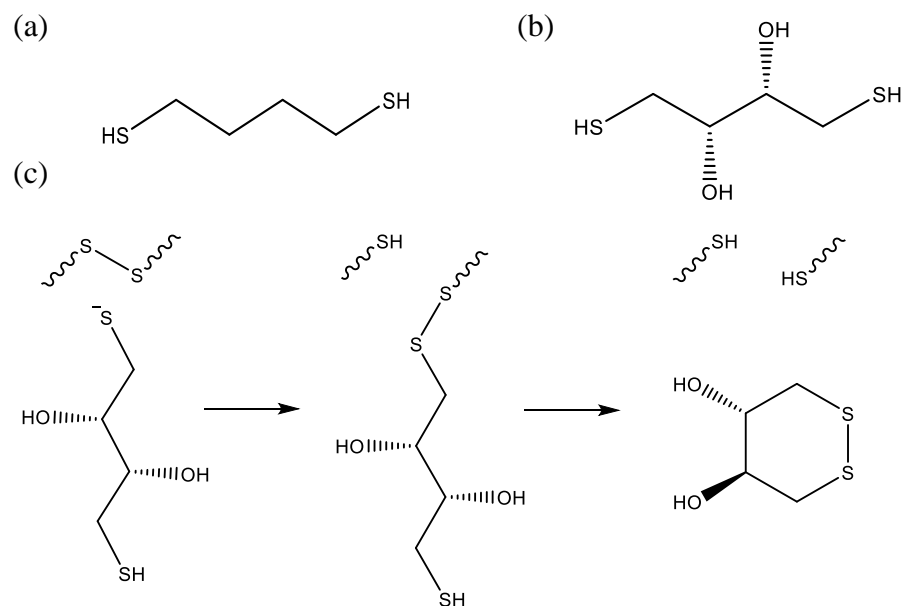


Figure 14. The structures of the two reducing agents, DTB (a) and DTT (b). (c) shows reduction of disulfide bonds by DTT, which itself oxidizes.⁴⁴

In this study we tested the structurally similar reducing agents DTT as well as DTB to prevent the formation of disulfide bonds and ensure a smooth surface topography of PMMS prior to PEGylation. DTT differs from DTB in that it has two hydroxyl groups in the middle carbons.

1.6 Surface characterization techniques

1.6.1 *Contact angle goniometry*

A common surface characterization technique to determine the extent of hydrophilic or hydrophobic nature, in other words wettability, of a solid surface is contact angle goniometry. When a surface is wetted with a single drop of a liquid, the shape of the drop on surface is dependent on factors such as the air/vapor surrounding it, the properties of the surface as well as the properties of the drop itself. This can be described by Young's equation which is essentially a function of the interfacial tensions (eq. 1).⁴⁶

$$\gamma_{sl} + \gamma_{lv} \cos \theta = \gamma_{sv} \quad (1)$$

Here γ_{sl} , γ_{lv} and γ_{sv} denote the interfacial tensions between the solid and the liquid, the liquid and the vapor and the solid and the vapor, respectively, and θ is the equilibrium contact angle that is formed by the intersection of the liquid-vapor and solid-liquid interfaces (Figure 15). Essentially, it is the angle between the tangent at the contact line along the liquid-vapor interface and the x-axis. Figure 15 shows various instances of contact angles. An acute contact angle implies that the liquid spreads over a large area of the surface, which is hydrophilic. An obtuse contact angle, on the other hand, would indicate that the wetting of the surface is not favorable, hence the liquid would form a compact droplet by minimizing its contact with the surface.⁴⁷

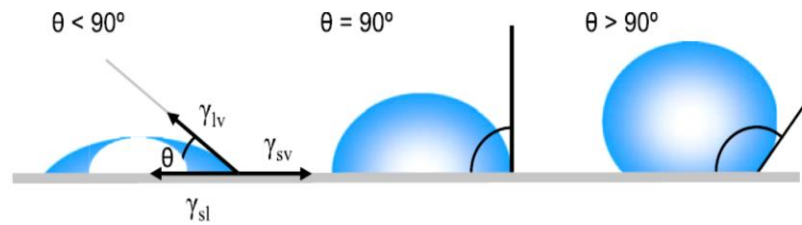


Figure 15. Cases of the extent of wettability of the surface as shown by the values of the contact angle.⁴⁷

Although eq. 1 describes the possibility of only one contact angle, liquid drops typically have a range of contact angles from the advancing contact angle (θ_A), a maximum value, to the receding contact angle (θ_R), a minimum value. They can be determined by adding and withdrawing the liquid droplet on a substrate, respectively. Wetting is not a static state. Apart from the surface tensions there is another factor that contributes to the total energy of the system which determines the shape of the drop. This is the line energy associated with the three-phase contact line and is the result of the inconsistencies in the smoothness of the surface, which can be chemical or physical. Thus, there can be differences in values of the line energy at different regions depending on the inconsistencies or the defects of the surface which act to pin the contact line. This pinning results in contact angle hysteresis which is the difference between θ_A and θ_R . This is the underlying concept of dynamic contact angles, which can be measured at various speeds.^{47, 48} In this study, we measured the dynamic contact angles to quantitatively determine the extent of hydrophilization of the PEGylated PMMS substrate.

1.6.2 Atomic force microscopy

In the 1980s, a powerful instrument, which allowed the imaging of the topography of insulating and conducting surfaces on the order of fractions of a nanometer, i.e. with atomic resolution, was made commercially available. This instrument, the atomic force microscope (AFM), belonged to a series of scanning probe microscopes invented around the same time.⁴⁹

Figure 16 shows the basic components of the AFM system. AFM consists of a micro-fabricated cantilever made of silicon or silicon nitride with a sharp tip that is able to scan the surface of interest. The deflection or oscillation amplitude of the tip is measured as it scans the surface, hence information regarding the topography is obtained. These measurements are attained with an optical tracking system that uses a photo-detector to track the reflection of a laser or a superluminescent diode off the back of the cantilever. These detected changes in position of the cantilever are corrected to a set point value by means of a feedback controlled piezo which adjusts the tip to sample distance. The correction voltages are sent to the Z piezo, followed by recording and correlating of data in order to determine the height at a given XY coordinate. Inconsistencies due to hysteresis, drift, creep and gaining effects are accounted for by sensors so as to measure the actual piezo actuation in XYZ coordinate system.^{49, 50}

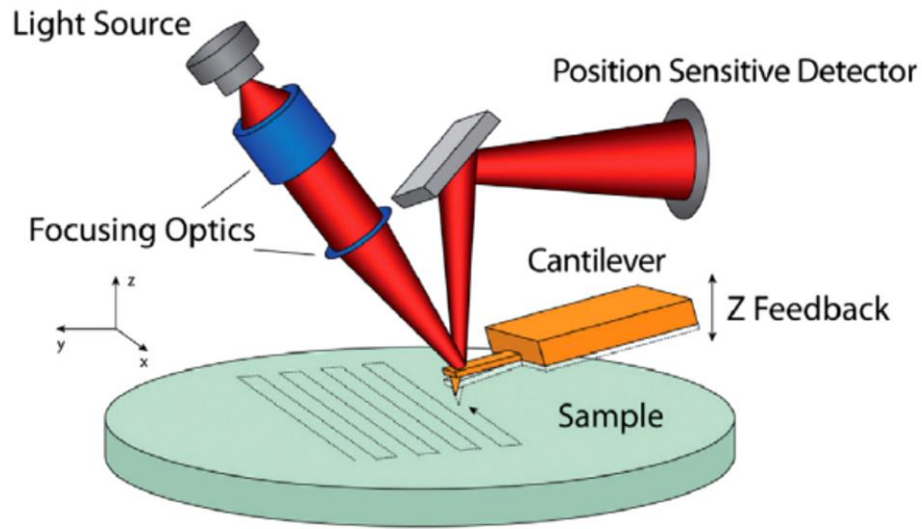


Figure 16. Scheme depicting the components of the topography detecting system of an AFM.⁵⁰

Three scanning modes have been employed in AFM: contact, non-contact and tapping mode. In the contact mode, the tip of the cantilever is dragged across the surface of interest and produces the topographical map. Although this technique has been successfully implemented in some cases, typically concerns such as damage to the tip and sample as well as creation of artificial features on the acquired images arise due to the dragging motion of the probe tip coupled with adhesive forces between the surface and the tip. The non-contact mode overcomes such issues by placement of the tip at a small distance above the sample, thereby avoiding direct contact between the tip and the surface. Again, this technique also results in drawbacks such as low resolution of images, unusable data and damage to samples since in this case the probe is frequently drawn to the surface by the surface tension of any

adsorbed liquids on the sample. The limitations of contact and non-contact modes are overcome by use of tapping mode, as done in our experimentation. In the latter case, the tip is alternately placed in contact with the surface and lifted from it while oscillating at or near the resonance frequency. The amplitude of oscillations is adjusted according to whether the tip is in contact with the surface or not by a constant feedback loop. This ensures a high resolution image while avoiding dragging across the surface of the sample. The oscillating cantilever operating in tapping mode is able to overcome frictional and shear forces otherwise experienced by the samples in contact and non-contact modes and also provides a large linear operating range, stabilizing the vertical feedback system to a great extent.⁵¹

II. EXPERIMENTAL

2.1 Materials and Apparati

General. Silicon wafer substrates (100 orientation, P/B doped, resistivity 1-10 Ω -cm, thickness 475-575 μ m) were purchased from International Wafer Service, Inc. Mercaptopropylmethylsiloxane dimethylsiloxane copolymers (SMS 042 containing 4%-6% -SH group), mercaptopropylmethylsiloxane homopolymer (SMS 992 containing 100% -SH group) and allyloxy (polyethylene oxide) (8-12 EO) were purchased from Gelest. Photo-initiator 2-hydroxy-2-methyl-1-phenyl-propan-1-one (Darocur 1173 Ciba®) was purchased from Ciba Specialty Chemicals. DL-Dithiothreitol (\geq 98% by TLC, \geq 99% by titration), 2-allyloxyethanol (-98%), bovine serum albumin (BSA; A-3912; >96% protein) and lysozyme from chicken egg white (\geq 90% protein) were purchased from Sigma-Aldrich. All organic solvents (toluene, acetone, and reagent alcohol) were purchased from Fisher Scientific, Inc. Water used was purified using Millipore Milli-Q Biocel System (Millipore Corp).

Instrumentation. All silicon wafers were oxidized in a Harrick plasma cleaner PDC-001 (Harrick Scientific Products, Inc.) prior to grafting reactions. Ultra-violet light irradiation was completed using UV collimated light source

Model 30, along with a constant intensity controller, and a model 150 shutter timer (OAI Inc., CA). Thickness measurements were carried out with an LSE Stokes ellipsometer (Gaertner Scientific) equipped with a 1 mW He-Ne laser (wavelength 632.8 nm). Contact angles were measured using a NRL C.A 100-00 goniometer (Rame-Hart Instrument Co.) with a Gilmont Syringe (Gilmont Instrument Co.) attached to a 24-gauge flat-tipped needle. Milli-Q water was the probe fluid. Atomic force microscopy images were obtained with a Veeco Metrology Dimension 3100 Atomic Force Microscope (AFM) with a silicon tip operated in tapping mode. Image analysis was conducted in Nanoscope software (Veeco Instruments, Inc.).

2.2 Methods

Preparation of reduced SMS 992 solution. 1.5 wt %, 3.0 wt %, 6.0 wt % and 12.0 wt % of DTT and DTB solution was prepared by introducing 15 mg, 30 mg, 60 mg and 120 mg of DTT or DTB into 2 mL Eppendorf microcentrifuge tubes, respectively. 1 mL of SMS 992 and 0.5 mL of acetone were added subsequently to the tubes containing DTT while 1 mL of SMS 992 was added to the tubes containing DTB. This was followed by vortexing for 30 s.

Preparation of thiol-functionalized substrates by grafting of SMS 042 and SMS 992 onto oxidized silicon wafers. Silicon wafers were diced into 1.5 x 1.2 cm samples. Dust particles were removed by rubbing and rinsing thoroughly with distilled water followed by drying with compressed air. The wafers were left in a clean oven to dry for 30 min at 110 °C, after which they were cleaned in a Harrick oxygen plasma cleaner at approximately 300 mTorr for 15 min. This ensured the removal of any organic impurities on the wafers. The cleaned wafers were placed in clean scintillation glass vials. Reaction was performed by drop-casting 100 μ L of SMS 042 or SMS 992 solution containing DTT onto each wafer with a micropipette. The tightly capped vials were placed in a heating block at 100 °C for 24 h. After completion of the reaction, the wafers were held using tweezers, rinsed thoroughly with toluene, acetone and Milli-Q water (in that order) followed by drying under a stream of nitrogen gas. The treated wafers were left in a desiccator overnight.

Preparation of PEG-grafted thiol-functionalized substrates. PEG solutions of different molecular weights were separately prepared in scintillation vials by vortexing together approximately 20% PEG, 80% ethanol (by volume) and 1 wt % Darocur-1173 as a photo-initiator. Wafers were placed in a polystyrene petri dish and a pipette was used to transfer the prepared PEG solution such that the wafers were completely submerged under the solution. The petri dish was covered with a clean, transparent glass cover and irradiated

for 999 s under a photolithography unit at 365 nm. Tweezers were used to remove the wafers, which were then rinsed thoroughly with ethanol and Milli-Q water sequentially and dried under a stream of nitrogen gas. The treated samples were left in a desiccator overnight.

Adsorption of model proteins on PEGylated substrates. PEGylated wafers were soaked in phosphate buffer saline (PBS, pH = 7.4) for 2 h, followed by immersion in 1 mg/mL albumin or lysozyme solution in PBS and incubation at 37 °C for 1 h. Dilutions using PBS were performed (3x) while keeping solution level above wafer surfaces at all times followed by agitation of the wafers in a beaker containing Milli-Q water. The samples were thoroughly rinsed with Milli-Q water before being stored in a desiccator overnight.

2.3 Surface Characterization

Atomic force microscopy. The topography of sample surfaces, i.e. the extent of roughness, was determined by using AFM tapping mode. A silicon tip (Veeco) was used which was routinely auto tuned before scanning the surface of the samples. Images of sizes 5×5 μm and 1.25 x 5 μm were captured with a data scale of 10 nm. The root mean square (RMS) value was recorded as an indicator of surface roughness after flattening and correcting for scan lines.

Contact angle goniometry. Advancing and receding contact angles were measured at three random spots on each sample. A total of 10 dynamic measurements were taken for advancing or receding contact angles at 0.5 s intervals. Contact angle measurements played an essential role in determining the extent of hydrophilicity of the PEGylated surfaces.

Thickness measurement by ellipsometry. Thickness was measured for each of the samples by placing the sample on the stage of the ellipsometer and measuring for thickness of silicon oxide and polymer layers at three different points.

III. RESULTS AND DISCUSSION

3.1 Fabricating a PMMS grafted platform for subsequent PEGylation

Overview. Silicon wafers were first grafted with SMS 042 or SMS 992 to prepare PMMS substrates for PEGylation (Figure 17). The two compounds, SMS 042 (5 % thiol groups) and SMS 992 (which has 99-100 % thiol groups), offer an insight as to how the concentration of thiol groups on the surface of the substrate affects the degree of PEGylation. Thiol-ene “click” chemistry, allows the grafting of PEG, i.e. EG and OEG layers, onto the PMMS surfaces thus altering the native PMMS surface topography and the extent of hydrophilicity. As discussed in Section 1.3, we used the protein repelling nature of PEG to hydrophilize the PMMS surface, where the molecular weight of EG and OEG or the chain length is used to tune protein resistance.³⁵ The effectiveness of EG and OEG to hydrophilize a surface was compared. Contact angle goniometry, ellipsometry and AFM imaging were analyzed so as to compare the two types of PMMS substrates and the (O)EG layers. The advancing and receding dynamic contact angles are primarily indicative of the extent of hydrophilicity of the surfaces. Of the two PMMS substrates, the platform that displays the most hydrophilicity was chosen for subsequent experimentation.

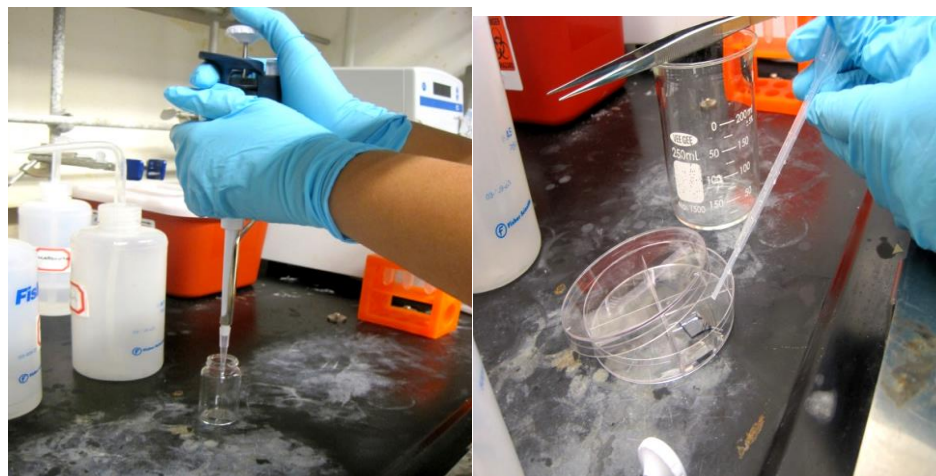


Figure 17. Drop-casting of PMMS to prepare thiol-functionalized substrates (left). Immersing PMMS-grafted substrates under PEG solution (right).

3.1.1 Comparisons between PMMS substrates

Thickness, contact angle and RMS (obtained from AFM images) values were compared for the two PMMS substrates (Table 1). Both advancing and receding contact angles of SMS 042 were observed to be greater than that of SMS 992. This can be attributed to the fact that SMS 992 has a much higher concentration of thiol groups (100 %) than SMS 042, which only has 5% thiol groups. SMS 042, which is a PDMS-PMMS copolymer, is not as hydrophobic as native PDMS and is a somewhat hydrophilic surface as indicated by the lower receding angle in particular. However, SMS 992 can be intuitively thought of as a surface consisting of only thiol groups and has significantly lower advancing as well as receding contact angles. Thus, SMS 992 offers a more hydrophilic surface than does SMS 042.

Table 1. Comparisons between SMS 042 and SMS 992 grafted silicon wafers in terms of contact angle, thickness and AFM RMS values.

	Contact angle (θ_A^0 / θ_R^0)	Thickness (\AA)	AFM RMS (\AA)
SMS 042	102 \pm 1/84 \pm 4	38 \pm 2	11 \pm 2
SMS 992	82 \pm 1/45 \pm 2	30 \pm 4	6 \pm 2

SMS 042 surfaces were typically observed to be thicker and rougher than SMS 992 surfaces. The white spots on the AFM height images (Figure 18) are areas with higher features. More occurrences of spots indicate a rougher surface. A possible explanation for the greater roughness and thickness of SMS 042 may be due to the fact that it is a PDMS-PMMS copolymer. This causes less surface homogeneity compared to SMS 992 which is a homopolymer.

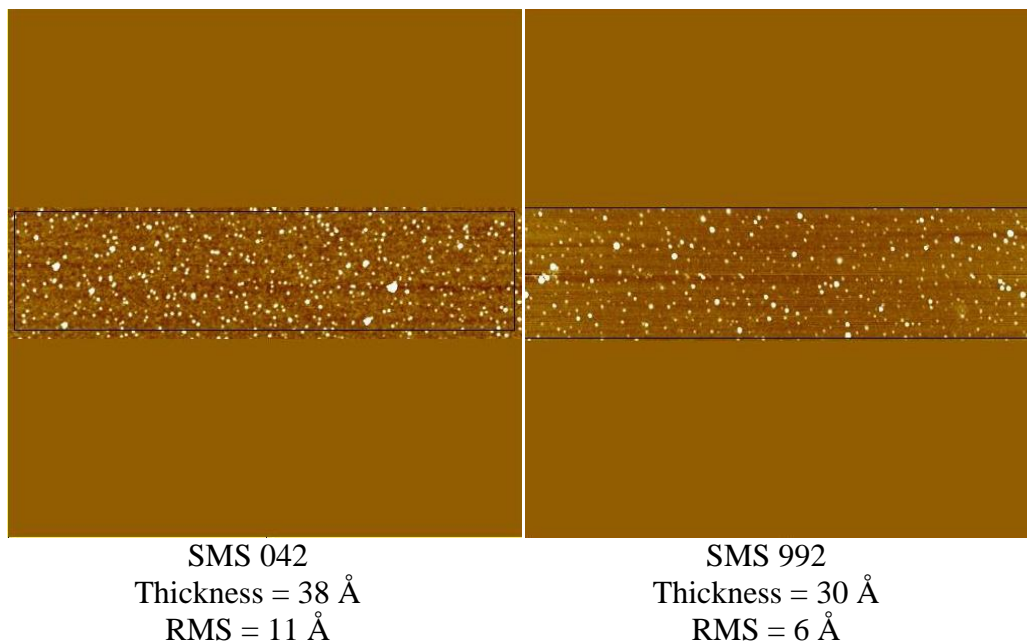


Figure 18. AFM images (size: 5 μm x 5 μm ; height: 10 nm) of SMS042 and SMS992 samples; SMS042 is rougher than SMS992.

However, upon further experimentation and observation of more SMS 992 substrates, it was observed that the topography, i.e. roughness, can vary from sample to sample (Figure 19). The topographies of the sample substrates ranged from completely smooth (RMS = 1 Å) to significantly rougher (RMS = 8 Å). This non-uniformity of the substrates was the likely result of disulfide aggregate formation (as discussed in Chapter 1). Formation of disulfide aggregates caused the surface to have seemingly random topographies and distorted the surface topographies of PMMS as well as subsequent PEGylated substrates.

It is noteworthy that AFM images are often distorted with scan lines and humidity effect, in addition to white background spots. The AFM is highly sensitive and humidity plays a significant role in the imaging process. Higher humidity levels have been shown to increase adhesion forces and reduce resolution of the images.⁵² The AFM tip is made of silicon and has a native oxidized layer, similar to the silicon wafers. Hence, these surfaces are hydrophilic which means that they attract water to form a layer. The thickness of this water layer may depend on relative humidity. As a result, the samples may have absorbed or adsorbed water, depending on surface hydrophilicity, because in addition to the silicon oxide layer, the PEG and thiol layers are hydrophilic too. This would ultimately result in larger surface features. In addition to that, the water layers on the tip and the sample surface can produce more attractive forces, hence changing the size of the surface features.

Keeping such considerations in mind, we decided to incorporate a reducing agent into this system, which will be discussed in Section 3.2.

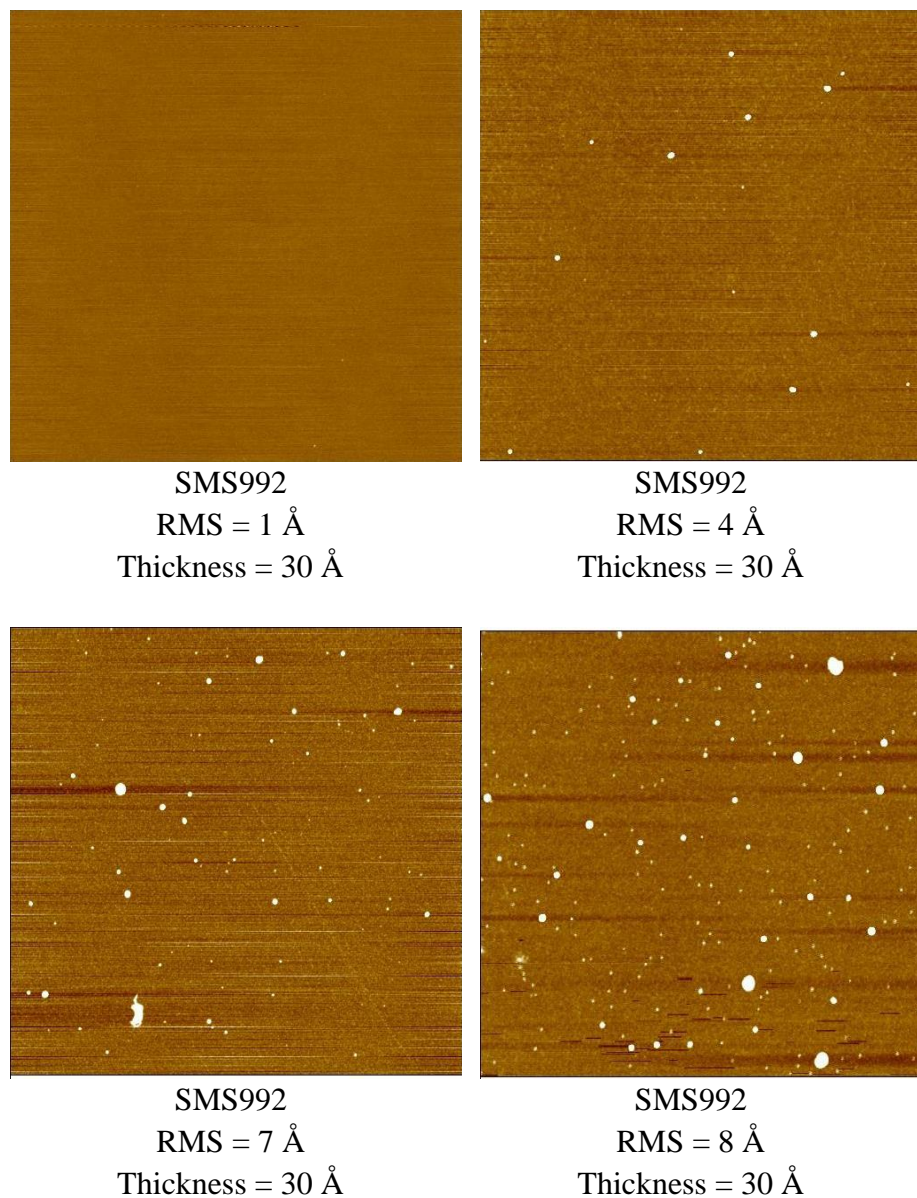


Figure 19. AFM images (size: 5 μm x 5 μm ; height: 10 nm) showing the varied topographies of SMS 992 samples.

3.1.2 Comparisons between EG and OEG to effectively hydrophilize PMMS substrates

The dynamic contact angles and thicknesses of the EG and the OEG layers grafted on SMS 042 and SMS 992 were compared. In the case of SMS 042, the thickness values for both EG and OEG layers were negligible; the negative thickness value of -5 \AA is the result of experimental and instrumental errors. In the case of SMS 992, however, although the EG layer was very thin, $\sim 1 \text{ \AA}$, the OEG layer was significantly thicker at 24 \AA . This coincides with the notion that OEG has a much longer chain length than EG.

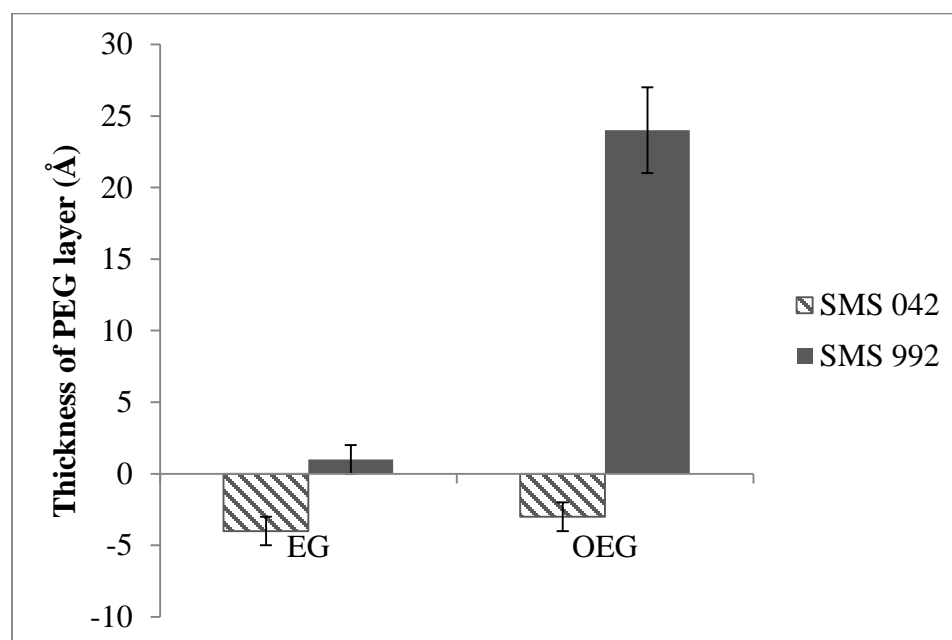


Figure 20. A comparison between the thickness of the (O)EG and OEG layers on SMS 042 and SMS 992.

Upon looking at the dynamic contact angle values (Figure 21) for the SMS 042 series, it is evident that the advancing contact angles do not change much

upon the incorporation of the EG or the OEG layer. The receding contact angles decrease upon the addition of the EG layer and fall even further in the case of the longer OEG layer, implying that the SMS 042 surface is hydrophilized to some extent upon the grafting of (O)EG layers. Intuitively, this is a reasonable phenomenon, owing to the fact that SMS 042 is a copolymer consisting of the mostly hydrophobic methyl groups of the PDMS as well as some hydrophilic thiol groups, where the “click” reaction of grafting of EG and OEG occurs. Hydrophilization is observed to a greater extent for SMS 992 as indicated by the lower advancing and receding contact angles upon grafting of EG. The dynamic contact angles further decrease in the case of OEG. This reduction of the dynamic contact angles in the case of SMS 992 is explicable by the fact that SMS 992 has a greater concentration of thiol groups allowing full coverage of EG or OEG groups via the “click” reaction. OEG in both cases is able to hydrophilize the surfaces of both SMS 042 and SMS 992 to a greater degree than EG, implying that chain length plays a significant role as discussed in Section 1.4. The difference in the advancing and the receding contact angles, i.e. hysteresis, increases in the case of SMS 042 indicating a more heterogeneous surface while the hysteresis decreases in the case of SMS 992 indicating a more homogeneous surface. Again, this heterogeneity of SMS 042 may be due to the PMMS-PDMS copolymer resulting in a non-uniform grafting of EG and the OEG. In

contrast, the SMS 992 surface offers a more uniform platform for the PEGylation to occur.

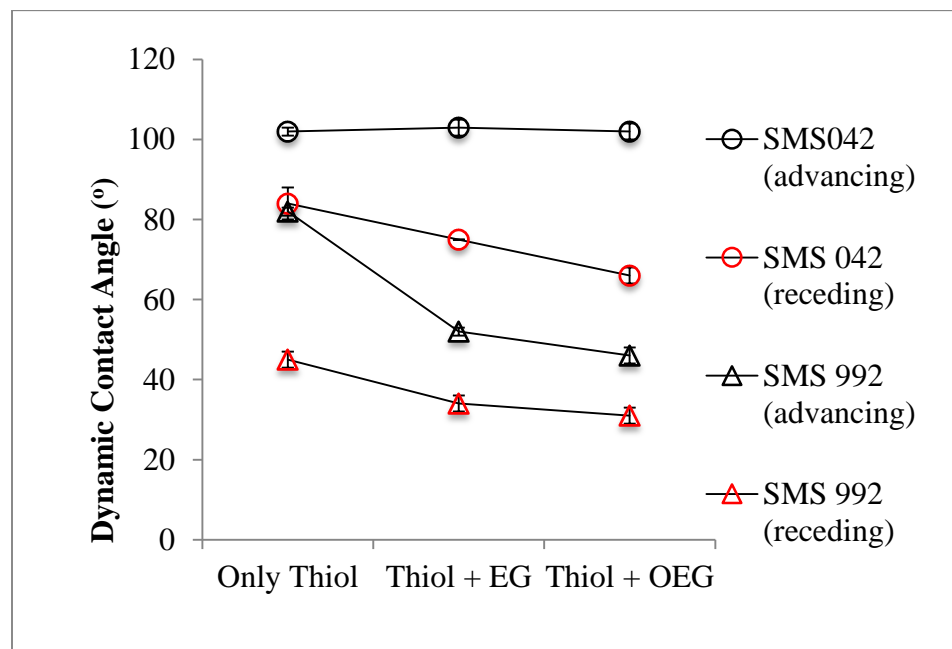


Figure 21. A comparison between the contact angles of SMS 042 and SMS 992 upon the grafting of PEG layers.

As seen in the AFM images (Figure 22) and accompanying RMS values (Figure 23), SMS 992 grafted with OEG is a much rougher surface compared to SMS 992 grafted with EG. Grafting of EG does not affect the surface of the SMS 992 significantly. OEG has a longer chain length than EG which effectively contributes towards a rougher surface.

Thickness and contact angle analyses of SMS 042 and SMS 992 before and after PEGylation directed towards SMS 992 as a better choice for a biocompatible platform. The low concentration of thiol groups proves as a limitation in this experimentation. However, the roughness of SMS 992 renders non-uniform grafting of PEG and difficulties in visualization of

subsequently adsorbed proteins. Therefore, in the rest of the studies, SMS 992 was first smoothed to ensure homogeneity of the substrate before further hydrophilization could be achieved by the grafting of PEG and protein adsorption studies.

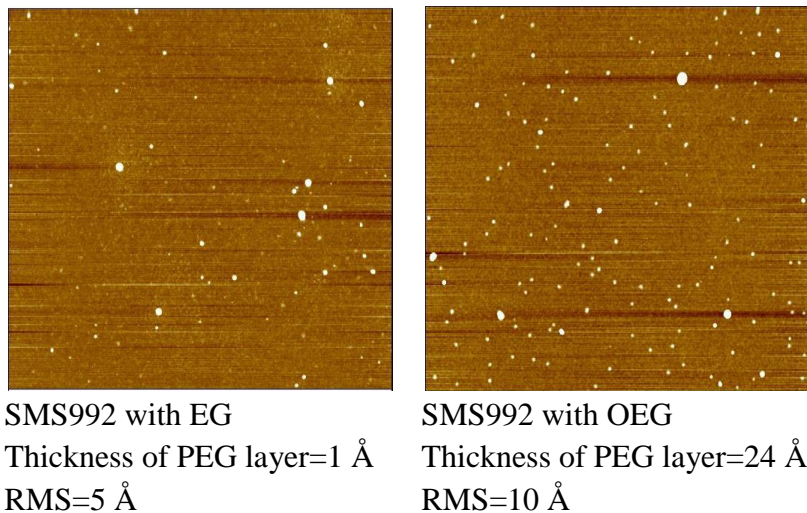


Figure 22. AFM images (size: 5 x 5 μm ; height: 10 nm) of SMS 992 grafted with (O)EG.

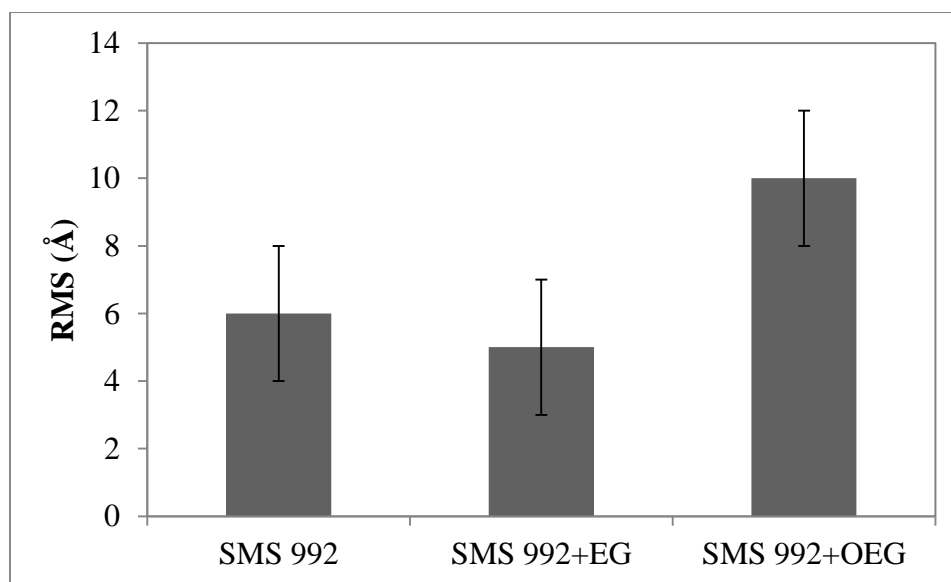


Figure 23. A comparison between the RMS values obtained from AFM imaging of SMS 992 and SMS 992 grafted with (O)EG.

3.2 Fabricating a smoothened SMS 992 substrate for PEGylation.

Overview. Once SMS 992 had been decided as the more suitable PMMS substrate, we aimed to smoothen the topography of SMS 992 by using a reducing agent. As discussed in Section 1.5, the addition of a reducing agent was necessitated by the observance of disulfide aggregates in AFM images of SMS 992 samples. Two reducing agents, DTB and DTT were the chosen candidates to smoothen the SMS 992 surface prior to PEGylation. Different amounts of the reducing agents in SMS 992 were also tested. Of the two, the more effective reducing agent and its most optimal amount were chosen based on the thicknesses, dynamic contact angles and topography of the substrate surfaces. Ideally, the most suitable amount of the reducing agent would result in a decrease in the thickness of the SMS 992 layer due to the breakdown of disulfide bonds. A smooth SMS 992 surface would also display minimal aggregation i.e. white spots upon AFM analysis. The optimal amount of the reducing agent was added to the SMS 992 and subsequent PEGylation was carried out. Observable changes (with or without the optimal amount of the reducing agent) in thickness, dynamic contact angles and AFM RMS were noted. To the best of our knowledge, the addition of a reducing agent into such a system is a novel technique that ensures a homogeneous platform for subsequent derivatizations.

3.2.1 Comparisons between DTB and DTT as the more suitable reducing agent

Figure 24 charts the comparisons between the thicknesses of the substrates upon addition of increasing amounts of both reducing agents. In general, a drop in thickness is observed for both DTB and DTT. This is reasonable because the formation of disulfide aggregates increases the thickness of the native SMS 992 layer.

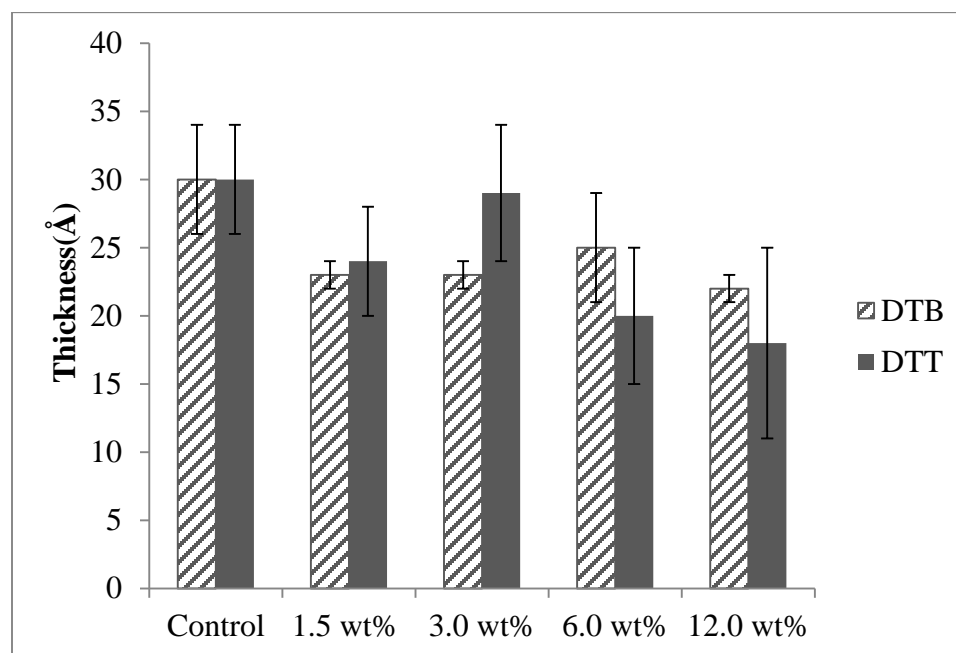


Figure 24. Changes in the SMS 992 layer thicknesses upon addition of increasing amounts of reducing agents, DTB and DTT.

Upon the addition of 1.5 wt % of DTB to SMS 992, the thickness decreased from 30 Å to 23 Å. Further increasing the amount of DTB did not alter the thickness much. Ultimately, 12.0 wt % of DTB resulted in 22 Å of SMS 992. DTT, on the other hand, yielded a more varying set of results. 1.5 wt % of DTT resulted in a thickness of 24 Å. Increasing the amount to 3.0 wt

% unexpectedly increased the thickness to 29 Å, which fell to 20 Å and 18 Å for 6.0 wt % and 12.0 wt %, respectively. The discrepancy in average thickness values is due to sample-to-sample and batch-to-batch variations and measurement errors. Furthermore, humidity levels affect the PMMS grafting reaction and the PMMS layer thickness. More accurate results would be obtained in a humidity-controlled environment, however, for the purposes of this experiment the mean values obtained are sufficient for understanding the topography of the reduced SMS 992.

Figure 25 shows that the dynamic contact angles do not vary upon addition of either reducing agents. Advancing and receding contact angles stay fairly constant for every amount of DTT or DTB and are similar to the observed dynamic contact angle values for the native SMS 992 surface. This implies that the reducing agents do not affect the nature or hydrophilicity of the surface. Interestingly, this also indicates that the disulfide aggregates do not affect the hydrophilicity of the SMS 992 surface.

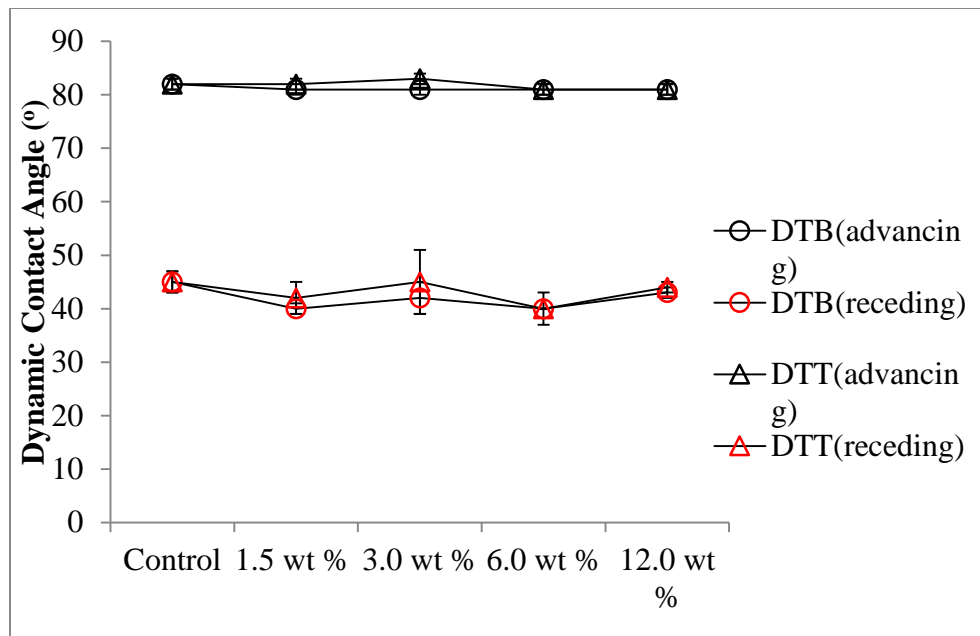
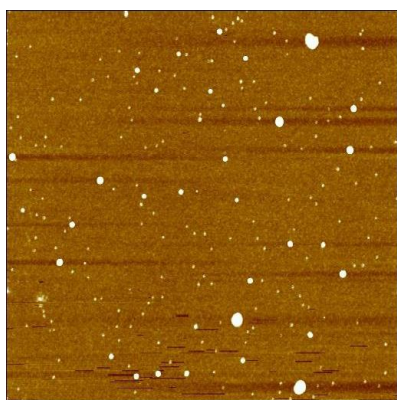
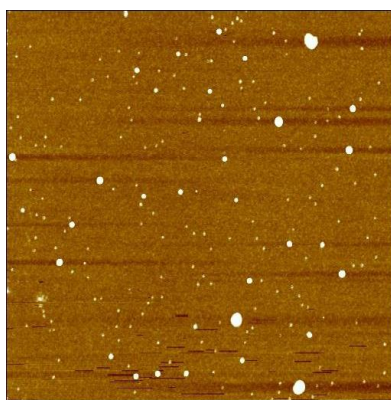


Figure 25. Constant contact angles of the SMS 992 layers upon addition of increasing amounts of reducing agents, DTB and DTT.

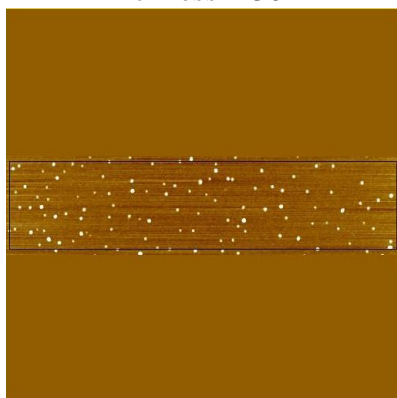
Inspection of the substrates using AFM revealed the changes in topography of SMS 992 layers upon the addition of DTT and DTB. These changes were quantified by the RMS values (Figure 27) while the AFM images (Figure 26) gave an overall idea of the topography. Both reducing agents were able to successfully smoothen the surface by preventing the formation of disulfide linkages as evidenced by the reduction in size and amount of the white spots as seen in the images as well as in the RMS values.



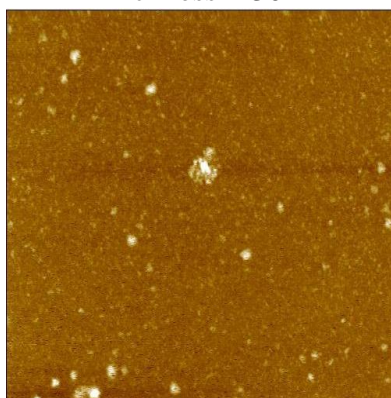
SMS992
RMS = 6 Å
Thickness = 30 Å



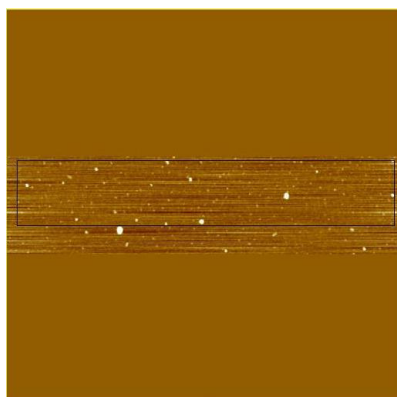
SMS992
RMS = 6 Å
Thickness = 30 Å



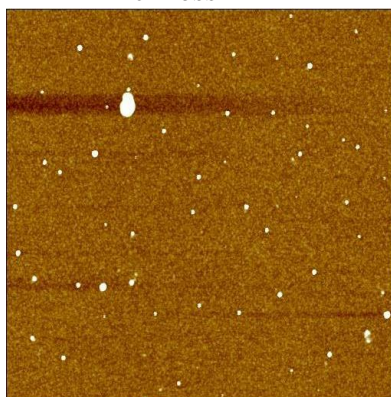
1.5 wt % DTB
RMS = 7 Å
Thickness = 23 Å



1.5 wt % DTT
RMS = 4 Å
Thickness = 24 Å



3.0 wt % DTB
RMS = 4 Å
Thickness = 23 Å



3.0 wt % DTT
RMS = 4 Å
Thickness = 29 Å

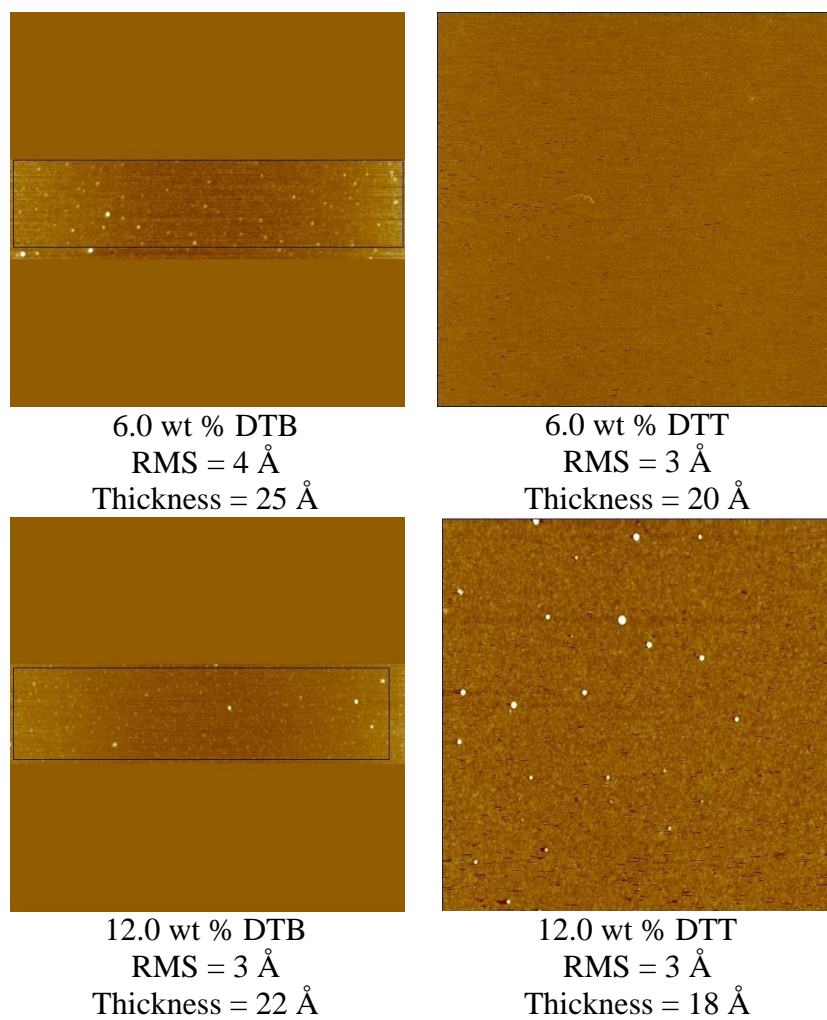


Figure 26. AFM images (size: 1.25 x 5 μm , 5 x 5 μm ; height: 10 nm) of SMS 992 layers comparing the resulting smoothness upon addition of varying amounts of DTB and DTT.

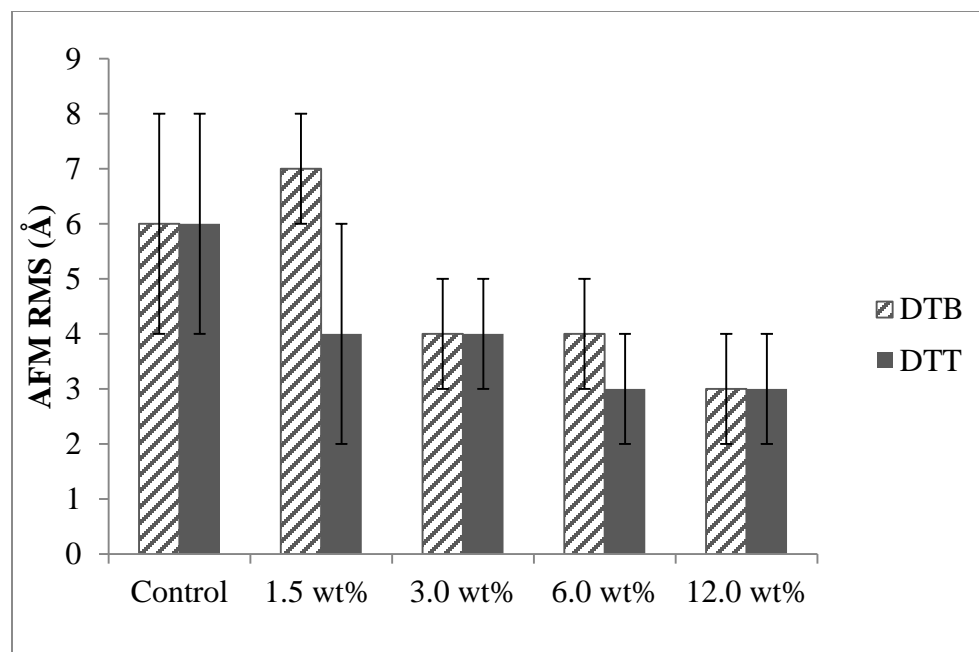


Figure 27. Changes in the RMS values of the SMS 992 layers upon addition of increasing amounts of reducing agents DTB and DTT.

Addition of 1.5 wt % of DTB did not alter the surface topography to a noticeable extent. However as the amount of DTB was increased to 3.0 wt %, 6.0 wt % and finally 12.0 wt %, the occurrences of the white background spots decreased as reflected by the drop in the AFM RMS values to 3 Å for 12.0 wt % of DTB. A similar trend was observed for DTT, where the first drop in the AFM RMS values was observed upon addition of 1.5 wt % of DTT (from 6 Å to 4 Å). The RMS value further decreased to 3 Å upon the addition of 6.0 wt % and a similar value was observed for 12.0 wt % of DTT. The AFM images again show a decline in the appearance of white spots and reveal that the surface is becoming smoother as more DTT is added. A discrepancy in the trend is seen in the case of 12.0 wt % DTT showing

reappearance of spots, which cannot be sufficiently explained. It is possible that excess DTT is difficult to rinse off leaving residues on the surface. In terms of contact angle, thickness and RMS values, we can conclude that 6.0 wt % of DTT and 12.0 wt % of DTB are similar in terms of effectiveness. However, upon closer inspection of the AFM images, we observe that in the case of DTB, while the larger white spots are reduced, much smaller spots are observed in the background. This implies that DTB, while reducing the disulfide linkages, may be forming aggregates on its own, which, although smaller in size, are nevertheless forming and distorting the topography of the SMS 992 surface. Such a phenomenon is not observed in the case of DTT, which even results in the smoothest, i.e. the most reduced surface, without any aggregates upon addition of 6.0 wt %. This type of smooth surface was observed consistently for other samples with 6.0 wt % DTT added. Accordingly, 6.0 wt % of DTT in SMS 992 was decided to be the optimal amount of reducing agent to be used for the subsequent steps of this study.

Additionally, a minor challenge that we faced during experimentation with DTB was the strong odor due to vapor pressure of the thiol-containing liquid. This issue was absent in the case of DTT solid, which proved as a convenience during our studies.

3.2.2 Effect of the addition of DTT to SMS 992 in subsequent PEGylation

Figure 11 compares the OEG and EG layer thicknesses with or without the addition of 6.0 wt % of DTT in SMS 992, i.e. the optimal amount of the chosen reducing agent. In the case of EG, the addition of the reducing agent increases the thickness of the EG layer from 1 Å to 7 Å. In contrast, for OEG, both the thicknesses, with or without the addition of reducing agents, are equal at ~24 Å. Looking at the molecular structures of EG and OEG, we can compare the value of thicknesses that we have obtained with the molecular chain lengths (Figure 28). Considering the average bond lengths and bond angles of all the bonds in our PEG molecule, the length of the projection approximately equals 1 Å for each of the bonds. This is the value that we use for an estimate of the molecular chain length. Hence, since EG has a total of 6 bonds, its molecular chain length approximately equals 6 Å. Similarly, since OEG has a total of 33 bonds, therefore its molecular chain approximately equals 33 Å. While the thickness of EG is comparable to its molecular chain length, OEG has a much higher molecular chain length value than its thickness. These differences intuitively seem reasonable. EG, is a much shorter chain than OEG and hence its actual thickness is similar to the theoretical molecular chain length. OEG, in contrast, is a longer chain length and may not be present in its stretched out, open chain form in reality.

Therefore, a smaller thickness value for OEG is expected.

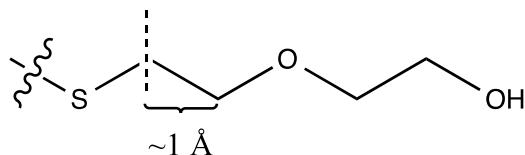


Figure 28. The approximate length of the molecular chain of EG. If the average bond lengths and bond angles of all the bonds are considered, the length of the projection approximately equals 1 Å.

A proposed explanation for the increase in the thickness of the EG layer lies in the fact that formation of disulfide bonds on the surface of the SMS 992 substrate would prevent PEGylation from occurring. Upon the addition of DTT, more free thiol groups are available for the thiol-ene chemistry to proceed, hence the thickness of the EG layer with DTT is higher than that without DTT. However, the same phenomenon was not observed in the case of the OEG layer, i.e. the addition of DTT does not seem to be affecting the thickness of the OEG layer, which implies that the reduction of the disulfide aggregates does not affect the extent of PEGylation. This challenges the proposed explanation in the case of EG where there is a difference in the EG layers with or without the reducing agent.

OEG, which has a much longer chain length than EG, naturally has a relatively high thickness where any difference caused by DTT is not seen. EG, on the other hand, being a shorter monomer, is more prone to variations caused by a reduction in the disulfide linkages. Again, it is possible that differences in the level of humidity and errors associated with experimentation

and instrumentation may have resulted in such changes in the thickness and in reality there is no significant change in the EG layers with or without DTT. Overall, therefore, we can conclude that while DTT is effective at reducing disulfide linkages and lowering the thickness of SMS 992, it does not seem to be affecting the extent of PEGylation even though it intuitively “frees up” disulfide linkages to offer more thiol bonds for PEGylation to occur.

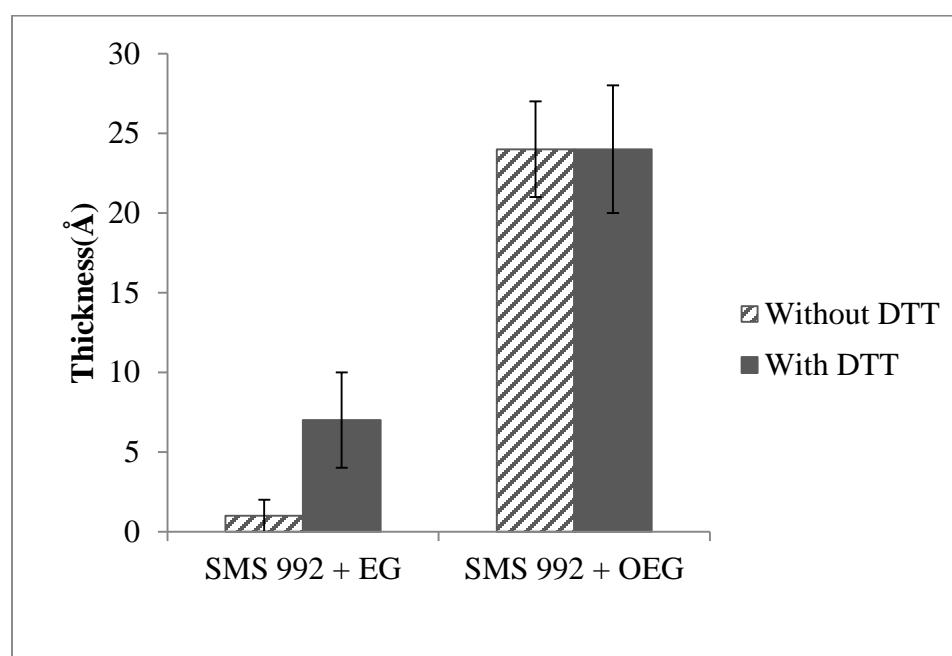


Figure 29. Comparisons of (O)EG layer thicknesses with and without the use of DTT as a reducing agent in the grafting of SMS 992.

Contact angles for EG and OEG layers do not vary significantly upon addition of DTT as shown in Figure 12. This again bolsters the fact that DTT does not play a role in changing the hydrophilicity of the SMS 992 surface and neither does it affect the surface hydrophilicity of the PEGylated substrates. This further implies that DTT is overall a good reducing agent that

does not tamper with the chemical nature of any surface, meaning that the protein repelling nature of the PEGylated substrates remains unaffected.

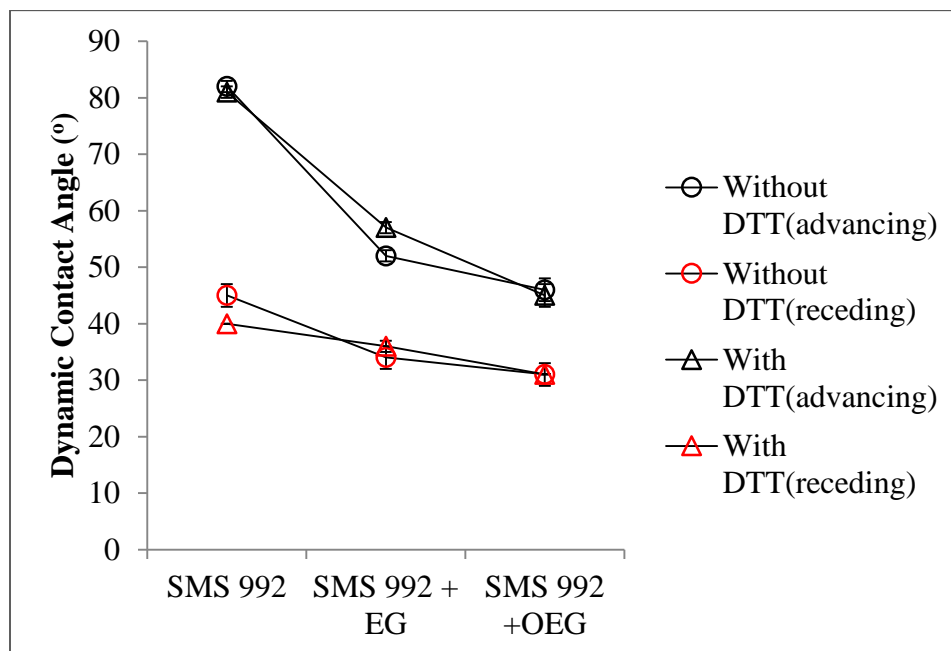


Figure 30. Comparisons of contact angles of (O)EG layers with and without use of DTT as a reducing agent in the grafting of SMS 992.

AFM images (Figure 13) and RMS values (Figure 14) provide more convincing evidence of the effectiveness of DTT as a reducing agent. The occurrence of white spots, i.e. aggregates, are reduced upon addition of DTT for EG as well as OEG substrates. EG substrates especially display a perfectly smooth and homogeneous surface when DTT is added which again implies that disulfide aggregates were formed without DTT. EG substrates are capable of showing completely smooth surfaces, similar to a reduced SMS 992 surface (Figure 9), because EG is a one-unit monomer with relatively low thickness and roughness. The RMS values of the EG layer upon addition of DTT drops

from 5 Å to 3 Å, similar to the surface of DTT-reduced SMS 992, meaning that previously, the roughness of the EG layer was distorted by disulfide aggregate formation. Similarly, the OEG layer, upon addition of DTT, also has a lower roughness and a decreased number of white spots in the AFM images, because the presence of disulfide aggregates again distorted the topography of the OEG layer. The OEG layer itself shows some white spots and a RMS of 8 Å because the OEG layer is a longer chain of 10 units which reasonably adds some roughness to the surface.

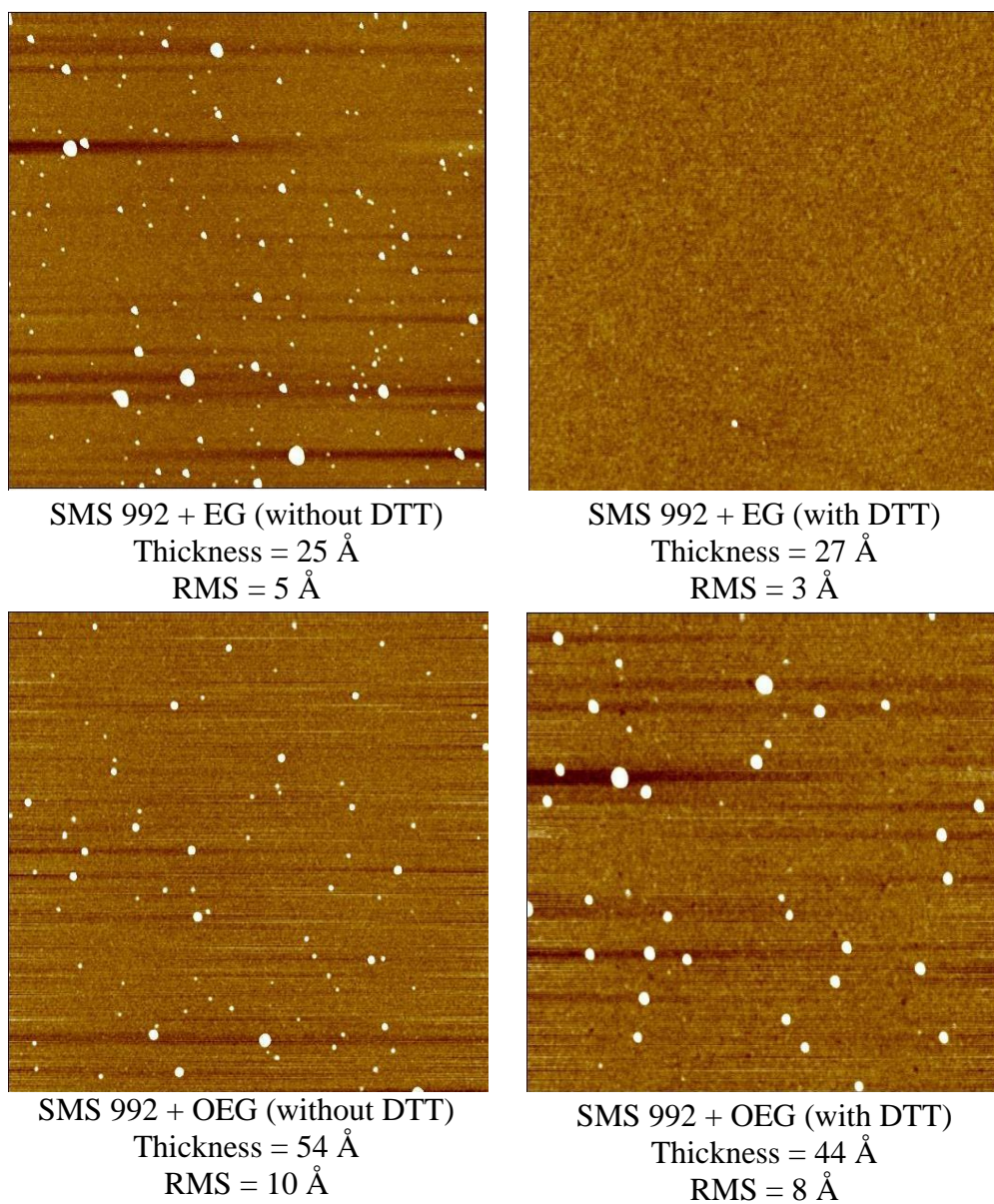


Figure 31. AFM images (size: 5 x 5 μm ; height: 10 nm) depicting that the addition of DTT to SMS 992 results in different topographies for the (O)EG layers.

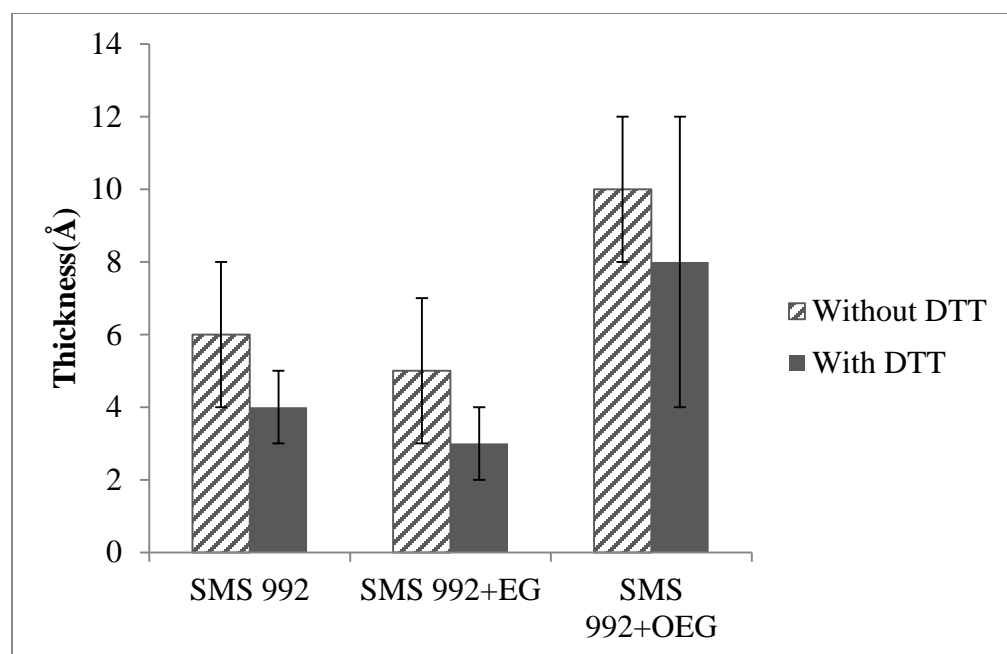


Figure 32: Comparisons of AFM RMS values of (O)EG layers with and without use of DTT as a reducing agent in the grafting of SMS 992.

Therefore, considering thickness, contact angles and AFM topographies in particular, we are able to validate the fact that 6.0 wt % of DTT in SMS 992 proves as an excellent reducing agent that does not affect the extent of PEGylation on SMS 992 while smoothening out and homogenizing the substrate to allow protein adsorption studies.

3.3 Effectiveness of PEGylated SMS 992 as protein repelling surfaces

Overview. Once a protein repelling platform was fabricated, we tested it for resistance towards proteins. As discussed previously, addition of the protein repelling PEG onto the SMS 992 platform should ideally result in no protein adsorption. The two proteins that were tested were bovine serum

albumin and lysozyme from chicken egg. Serum albumin is a protein which is responsible for carrying fatty acids in the blood and hence is abundantly found in the blood plasma.⁵³ Lysozyme is a small and stable enzyme which has the ability to attack the protective cell walls of bacteria and hence prevent bacterial infection.⁵³ Once again, contact angle goniometry, thickness ellipsometry and AFM imaging were used to evaluate the effectiveness of the platform for protein repulsion. The results obtained from these characterization techniques were compared for before and after protein adsorption. Primarily, no further increase in thickness values would be an indicator that protein has not attached onto the surfaces. Changes in dynamic contact angle values and AFM RMS would also be expected.



Figure 33: Preparation for protein adsorption studies by soaking in PBS prior to exposure to proteins (left). Incubation of the substrates in protein solutions (right).

3.3.1 Protein resistant surfaces

Figure 34 compares the thicknesses of the adsorbed albumin and lysozyme layers on SMS 992 and SMS 992 grafted with (O)EG layers. Substrates soaked in PBS were used as controls. It was seen that PBS, albumin and lysozyme result in increased thickness upon adsorption (18 Å, 26 Å and 40 Å, respectively) in the case of SMS 992. Surprisingly, soaking in PBS seems to be adding to the thickness of the native SMS 992 layer, which implies that the surface thiol groups must be interacting with solutes in PBS. This may also be due to solvent evaporation or changes in pH over time leading to precipitation of the PBS solutes. AFM images of the PBS-treated substrates display regions where precipitation may have occurred. Analyzing the thicknesses of SMS 992 with EG and SMS 992 with OEG soaked in PBS gave interesting results. Seemingly, soaking in PBS results in a negative value (-9 Å) for OEG. This means that the average thickness of PBS-treated OEGylated SMS 992 wafers is lower than that of native OEGylated SMS 992. This may possibly be a result of the dehydration of the OEG layer in a salty PBS environment. (O)EG surfaces are inherently hydrated with water and the presence of salts in PBS may result in the loss of water molecules from the (O)EG layers due to osmotic pressure. Molecular chain length may also be playing a role in the extent of dehydration, therefore, EG does not significantly display such a phenomenon while OEG does. As previously observed, OEG surfaces are more hydrophilic than EG surfaces.

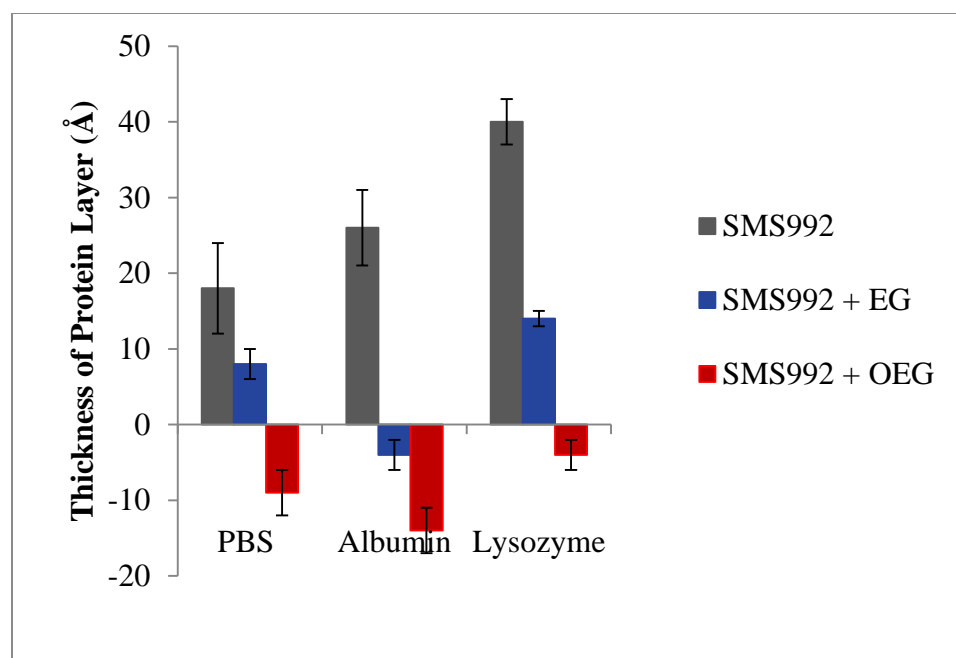


Figure 34. Comparisons of SMS 992 and PEGylated SMS 992 thicknesses before and after adsorption of PBS, albumin and lysozyme.

Although albumin is a bigger protein (molecular weight: ~66,500 Da)⁵⁴ compared to lysozyme (molecular weight: ~14,300 Da)⁵⁴ (Figure 35), its thickness on SMS 992 is lower than that of lysozyme on SMS 992. This can be explained by the structural differences between the two proteins. Albumin, which has two free cysteine residues in its structure, is able to interact covalently with the thiol groups on the hydrophilic surface of SMS 992 and hence attach itself effectively onto the surface of SMS 992 via disulfide linkages.⁵⁵ Lysozyme, on the other hand, does not contain any free cysteine residues and can nevertheless adsorbed onto the surface via a disulfide interchange reaction occurring between a surface thiol and a disulfide bond within the lysozyme molecule.⁵⁶ Because of its small size, it can potentially

penetrate into the SMS 992 layer causing the thickness to increase to a further extent.

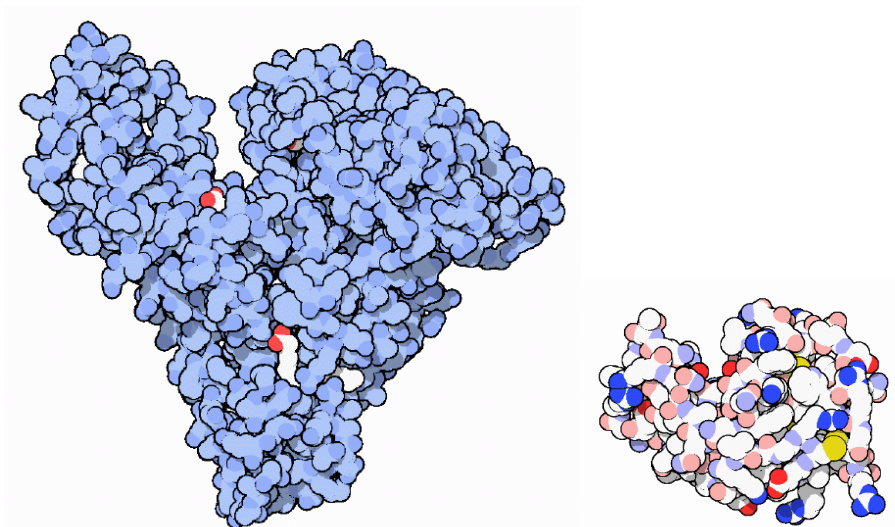


Figure 35. Structures of albumin (left) and lysozyme (right).⁵³ Albumin is a larger protein than lysozyme.

Another possible reason for the dissimilarities in the adsorption may be elucidated by the differences in charges of albumin and lysozyme. The isoelectric point, pI, of albumin is ~ 5 whereas that of lysozyme is ~ 11 .⁵⁴ In this study, PBS solution has a pH value of 7.4. At this pH, albumin is negatively charged whereas lysozyme is positively charged.⁵⁵ The C-S-H bonds are slightly polar due to the electronegativities of carbon, sulfur and hydrogen (Figure 17). Albumin, which is negatively charged, and lysozyme, which is positively charged, both encounter dipole-dipole interactions with the surface of the SMS 992. The differences in the nature and extent of charges of the two proteins may also contribute to the differences in the thicknesses of the protein layers. In addition to the covalent and dipole-dipole interactions,

hydrophobic interactions between the hydrophobic PDMS portion of the substrate and the hydrophobic portions of the proteins also give rise to the extensive protein adsorption on the SMS 992 substrate.

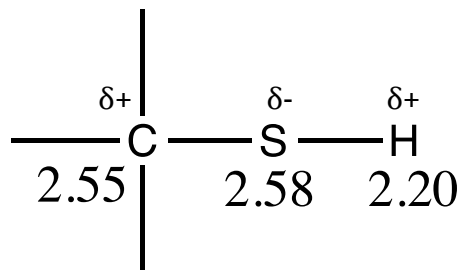


Figure 36. Electronegativity differences in the C-S-H bonds on the SMS 992 surface.

Figure 34 also shows that the thickness of the albumin layer drops to -4 \AA for EG and further drops to -14 \AA for OEG layers, implying that protein adsorption was successfully inhibited by PEGylation of the SMS 992 surfaces. Again, the negative thickness values, i.e. the fact that the thickness after protein adsorption was lower than the original PEGylated SMS 992 layer, could be attributed to the dehydration of the PEG layer in the presence of PBS. This validates the fact that PEGylation creates an excellent protein repellent platform. A similar trend is observed in the case of lysozyme where OEG reduces the protein layer to an even greater extent than EG.

Contact angle results further demonstrate the protein repellent ability of EG and OEG (Figure 37). Native SMS 992 has dynamic contact angles of $82^\circ/45^\circ$. After adsorption with PBS, albumin and lysozyme, the advancing contact angles of SMS 992 did not change much, however the receding contact angles significantly reduced to $\sim 11-14^\circ$ implying that the surface

chemistry has been altered and the surface contains additional species that are more hydrophilic than the $-SH$ moieties. However, on the EG and OEG surfaces, the advancing and receding contact angles after PBS, albumin and lysozyme adsorption remain at $\sim 50^\circ$ and $\sim 30^\circ$, similar to the values prior to adsorption. These results further reinforce that PEGylation alters the dynamic contact angles of the SMS 992 surface and PEGylated SMS 992 surface is protein resistant.

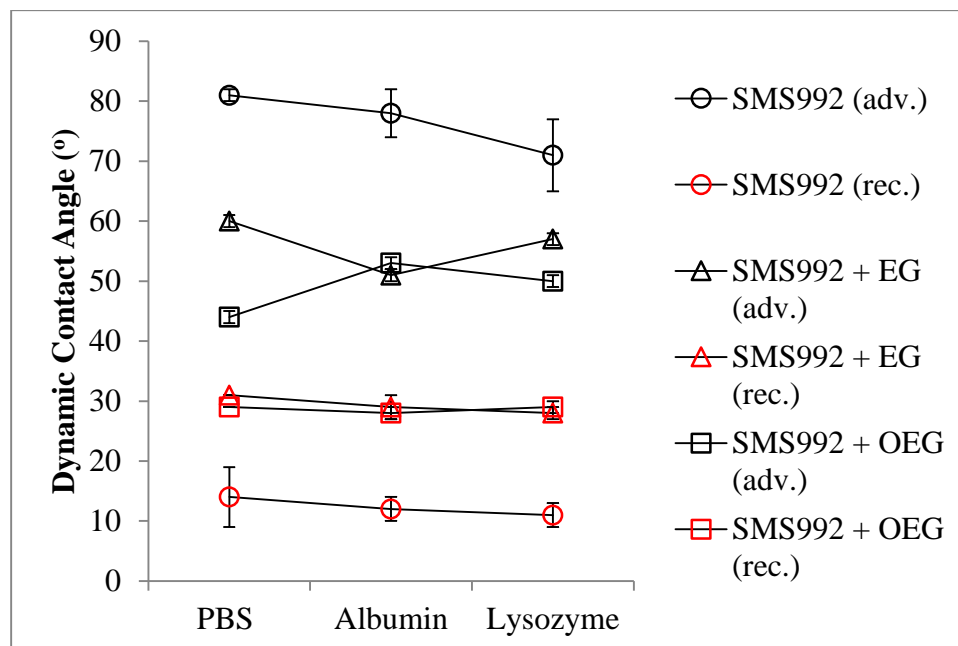


Figure 37. Comparisons of dynamic contact angles of SMS 992 and PEGylated SMS 992 before and after adsorption of PBS, albumin and lysozyme.

AFM images and RMS values, however, show some interesting features (Figures 38 and 39). PBS-treated samples seem to have regions containing precipitated solutes. Surprisingly, the RMS values of PBS-treated OEGylated SMS 992 samples are extremely high, which is likely to be due to the binding of

salts in PBS to the oxygen atoms in the OEG layers and/or insufficient rinsing of the substrates after PBS treatment. Substrates treated with albumin show some aggregation giving rise to greater RMS values and expectedly lysozyme-treated substrates show the most aggregation and the greatest RMS values. For albumin, upon incorporation of the EG layer, the surface shows less aggregation and even lesser aggregation in the case of OEG. This intuitively makes sense since the longer chain length of OEG is more effective at repelling proteins as discussed previously. Lysozyme, on the other hand, shows the most aggregation on EG layer (RMS value drastically increases to 65 Å). A reduction in the aggregates, i.e. fewer spots, is observed on OEG, where the RMS value is similar to the PBS-treated substrates. Lysozyme displays unexpected behavior, especially in the case of EGylated samples, for reasons that are not understood and we are working to find a reasonable explanation for this. Some of the discrepancies observed may be due to experimental errors. We plan to repeat the protein adsorption studies to minimize errors and to obtain more reproducible data.

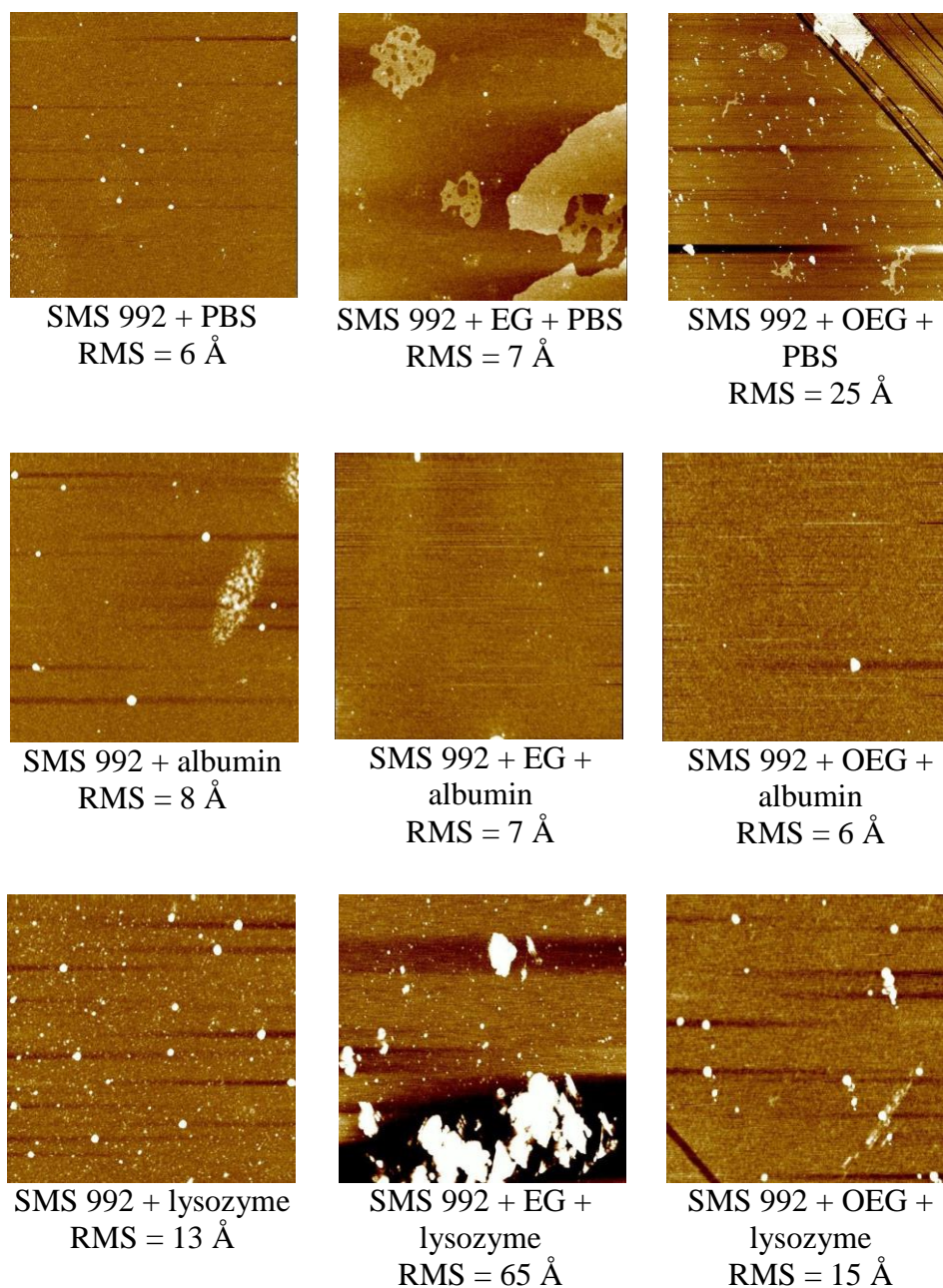


Figure 38. AFM images (size: 5 x 5 μm ; height: 10 nm) comparing the surface topographies of SMS 992 and PEGylated SMS 992 upon adsorption of PBS, albumin and lysozyme.

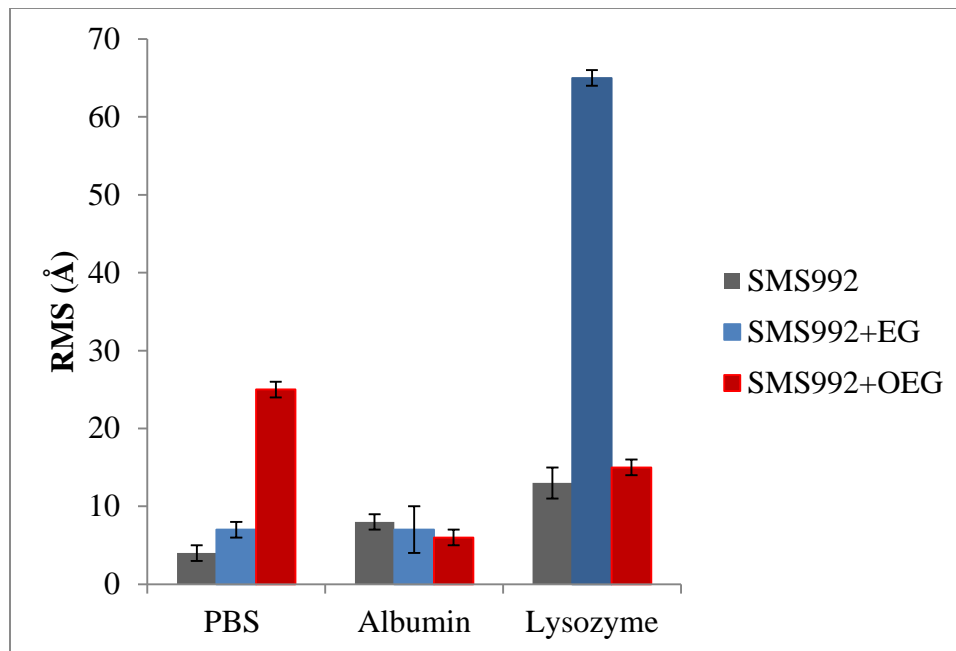


Figure 39. Comparisons of the AFM RMS values of SMS 992 and PEGylated SMS 992 before and after adsorption of PBS, albumin and lysozyme.

Even though AFM images and RMS values do not provide a clear picture, especially in the case of lysozyme, it is evident from the thickness and dynamic contact angle values that EG and OEG grafted SMS 992 substrates serve as excellent protein repellent surfaces. It should also be kept in mind that AFM images are representative of only micron-sized areas of the entire sample. The reproducibility of AFM imaging on a heterogeneous surface is difficult to attain. For lysozyme, it may be that the areas that we had chosen to scan had more aggregates compared to other areas and showed some interaction between the EGylated SMS 992 layer and the protein. In contrast, thickness and contact angle analyses present us with a macroscopic “average” view of the results and can be regarded as more reliable. Overall, the studies

on protein adsorption validate that our model, which can be reproducibly fabricated via a rapid technique, is effective as a biocompatible platform.

IV. CONCLUSIONS AND FUTURE WORK

A biocompatible platform was fabricated using a PDMS based substrate containing thiol groups (PMMS), a vinyl terminated PEG derivative and thiol-ene photochemistry. While comparing the PMMS substrates with different thiol concentrations on the surface, we observed that the compound with the higher concentration of thiol groups i.e. SMS 992 proved to be a better platform for subsequent PEGylation, for both cases of monomeric (EG) and oligomeric ethylene glycol (OEG), compared to the compound with the lower concentration of thiol groups i.e. SMS 042. Therefore, SMS 992 was the substrate of choice.

The thiol groups on the surface of SMS 992, however, participate in disulfide bond formation and result in aggregates which can be seen upon AFM imaging. This necessitated the incorporation of a reducing agent into the system that would ensure homogeneity of the surface, uniform grafting of PEG and a more accurate visualization of subsequently adsorbed proteins. Two reducing agents, DTT and DTB, were the chosen candidates and different amounts of these reducing agents were tested. Upon surface characterization, it was seen that overall DTT proved to a better candidate than DTB. While both reducing agents were successfully able to lower the roughness of the surface i.e. smoothen out the surface by reduction of

disulfide bonds, DTB seemingly showed miniscule aggregation in the topography which was visible upon keen observation of the AFM images.

This was absent in DTT reduced SMS 992 substrates. Next, the most optimal amount of DTT in SMS 992 was decided as 6.0 wt %. This amount was again chosen on the basis of results obtained upon surface characterization, in particular AFM analysis. It was observed that 6.0 wt % of DTT in SMS 992 resulted in a reproducibly smooth surface consisting of almost no aggregation. DTT, while successfully smoothening out the topography of SMS 992 and essentially “freeing up” –SH bonds for PEGylation, does not tamper with the hydrophilicity of the EG and the OEG. Thus 6.0 wt % of DTT proves to be a suitable reducing agent concentration that must be incorporated into the system.

Thiol-ene photochemistry was found to be an effective mechanism for the attachment of EG and OEG onto SMS 992, allowing us to take advantage of the reaction’s rapidity, resistance to oxygen inhibition, simplicity and reproducibility. OEG, because of its longer chain length, was a more hydrophilic surface than EG surface. Hydrophilization of the platform is an important criterion for biocompatibility i.e. protein repulsion.

To validate the model, protein adsorption studies were carried out on the EGYlated and OEGYlated substrates. Two commonly found proteins, albumin and lysozyme, were tested on SMS 992 –(O)EG substrates. While albumin showed promising results, lysozyme proved to be a trickier protein, especially

considering AFM analysis. This was attributed to structural differences in the two proteins. However, ellipsometry and goniometry results revealed that smooth and uniform SMS 992 grafted surfaces with both EG and OEG prove to be excellent protein resistant platforms, i.e. proteins were not adsorbed onto the surfaces.

These studies could be further explored by testing the biocompatible platforms on other commonly found proteins. Certainly, the structure and composition of the protein plays an important role, as evidenced by the differences that were observed with regards to the two model proteins of this experiment: albumin and lysozyme. Since humidity appears to cause some variations in data collections, the model could be tested in a humidity-controlled environment. Even longer ethylene glycol chains (for example, PEG with $n > 10$) could be tested which may perhaps lead to even better biocompatibility. Finally, data that elucidate the mechanical properties of this model could be obtained and coupled with our surface characterization results to form a device that is biocompatible in nature. Although our results are relatively small findings in the plethora of research directed towards PDMS-hydrophilization and PEGylation, we hope that this novel technique (which has not been implemented previously to the best of our knowledge) provides a simple and reproducible approach to fabricating a platform that is suitable for biological and biomedical applications.

REFERENCES

1. Nakanishi, K.; Sakiyama, T.; Imamura, K. On the adsorption of proteins on solid surfaces, a common but very complicated phenomenon. *J. Biosci. Bioeng.* **2001**, *91*, 233-244.
2. Rabe, M.; Verdes, D.; Seeger, S. Understanding protein adsorption phenomena at solid surfaces. *Adv. Colloid Interface Sci.* **2011**, *162*, 87–106.
3. Tirrell, M.; Kokkoli, E.; Bieskalski M. The role of surface science in bioengineered materials *Surf. Sci.* **2002**, *500*, 61–83.
4. Walker R. K., Krishnaswamy S. The activation of prothrombin by the prothrombinase complex. *J. Biol. Chem.* **1994**, *269*, 27441-27450.
5. Kalasin S.; Santore, M. M. Non-specific adhesion on biomaterial surfaces driven by small amounts of protein adsorption. *Colloids Surf., B* **2009**, *73*, 229-236.
6. Norde, W.; Gage, D. Interaction of bovine serum albumin and human blood plasma with PEO-tethered surfaces: influence of PEO chain length, grafting density, and temperature. *Langmuir* **2004**, *20*, 4162-4167.
7. Norde, W. Adsorption of proteins from solution at the solid-liquid interface. *Adv Colloid Interface Sci.* **1986**, *25*, 267-340.
8. Norde, W. Protein adsorption at solid surfaces: a thermodynamic approach. *Pure Appl. Chem.* **1994**, *66*, 491–496.
9. Estephan, Z. G.; Schlenoff, P. S.; Schlenoff, J. B. Zwitteration as an alternative to PEGylation. *Langmuir* **2011**, *27*, 6794–6800.
10. Holmlin, R. E.; Chen, X. X.; Chapman, R. G.; Takayama, S.; Whitesides, G. M. Zwitterionic SAMs that resist nonspecific adsorption of protein from aqueous buffer. *Langmuir* **2001**, *17*, 2841–2850.
11. Grey, J. J. The interaction of proteins with solid surfaces. *Curr. Opin. Struct. Biol.* **2004**, *14*, 110–115.

12. Colas, A.(eds); Curtis, J(eds). Silicone biomaterials: history and chemistry. Biomaterials Science: an introduction to materials in medicine 2nd edition. Ratner B. Elsevier Inc pp 80-86.
13. Graiver, D.; Farminer, K. W.; Narayan, R. A. Review of the fate and effects of silicones in the environment. *J. Polym. Environ.* **2003**, *11*, 129-136.
14. Zheng, P.; McCarthy, T.J. Rediscovering silicones: molecularly smooth, low surface energy, unfiled, UV/Vis-transparent, extremely cross-linked, thermally stable, hard, elastic PDMS. *Langmuir* **2010**, *26*, 18585-18590.
15. Krumpfer, J. W.; McCarthy, T. J. Rediscovering silicones: “unreactive” silicones react with inorganic surfaces. *Langmuir* **2011**, *27*, 11514-11519.
16. Krumpfer, J. W.; McCarthy, T.J. Contact angle hysteresis: a different view and a trivial recipe for low hysteresis hydrophobic surfaces. *Faraday Discuss.* **2010**, *146*, 103-111.
17. McDonald, J.C.; and Whitesides, G.M. Poly(dimethylsiloxane) as a material for fabricating microfluidic devices. *Acc. Chem. Res.* **2002**, *35*, 491-499.
18. McDonald, J. C.; Metallo, S. J.; Whitesides, G. M. Fabrication of a configurable, single-use microfluidic device. *Anal. Chem.* **2001**, *73*, 5645-5650.
19. Pinto, S.; Alves, P.; Matos C. M.; Santos, A. C.; Rodrigues, L.R.; Teixeira, J.A.; Gil, M. H. Poly(dimethyl siloxane) surface modification by low pressure plasma to improve its characteristics towards biomedical applications. *Colloids Surf., B* **2010**, *81*, 20–26.
20. Chen, H.; Brooke, M. A.; Sheardown, H. Silicone elastomers for reduced protein adsorption. *Biomaterials* **2004**, *25*, 2273–2282.
21. Bashir, R. BioMEMS: state-of-the-art in detection, opportunities and prospects. *Adv. Drug Delivery Rev.* **2004**, *56*, 1565– 1586.
22. Ng, J. M. K.; Gitlin, I.; Stroock, A. D.; Whitesides, G. M. Components for integrated poly(dimethylsiloxane) microfluidic systems. *Electrophoresis* **2002**, *23*, 3461–3473.

23. Whitesides, G. M. The origins and future of microfluidics. *Nature* **2006**, *442*, 368-373.
24. Bodas, D.; Khan-Malek, C. Formation of more stable hydrophilic surfaces of PDMS by plasma and chemical treatments. *Microelectron. Eng.* **2006**, *83*, 1227–1229.
25. Sharma, V.; Dhayal, M.; Shivaprasad, S.M.; Jain, S.C. Surface characterization of plasma-treated and PEG-grafted PDMS for micro fluidic applications. *Vacuum* **2007**, *81*, 1094–1100.
26. Kim, J.; Chaudhury, M.K.; Owen, M.J.; Orbeck, T. The mechanisms of hydrophobic recovery of polydimethylsiloxane elastomers exposed to partial electrical discharges. *J. Colloid Interface Sci.* **2001**, *244*, 200–207.
27. Flavel, B.; Jasieniak, M.; Velleman, L.; Ciampi, S.; Lúias, E.; Peterson, J. R.; Griesser, H. J.; Shapter, J. G.; Gooding, J. J. Grafting of poly(ethylene glycol) on click chemistry modified Si(100) surfaces. *Langmuir* **2013**, *29*, 8355-8362.
28. Kingshott, P.; Wei, J.; Bagge-Ravn, D.; Gadegaard, N.; Gram, L. Covalent attachment of poly(ethylene glycol) to surfaces, critical for reducing bacterial adhesion. *Langmuir* **2003**, *19*, 6912–6921.
29. Davis, F. F. The origin of peganology. *Adv. Drug Delivery Rev.* **2002**, *54*, 457-458.
30. Yu, Q.; Zhang, Y.; Wang, H.; Brash, J.; Chen, H. Anti-fouling bioactive surfaces. *Acta Biomater.* **2011**, *7*, 1550–1557.
31. Peppas, N. A.; Keys, K. B.; Torres-Lugo, M.; Lowman, A. M. Poly(ethylene glycol)-containing hydrogels in drug delivery. *J. Controlled Release* **1999**, *62*, 81–87.
32. Kim, P.; Kim, D. H.; Kim, B.; Choi, S. K.; Lee, S. H.; Khademhosseini, A.; Langer, R.; Suh, K.Y.; Fabrication of nanostructures of polyethylene glycol for applications to protein adsorption and cell adhesion. *Nanotechnology* **2005**, *16*, 2420–2426
33. Banerjee, I.; Pangule, R.C.; Kane, R. S. Antifouling coatings: recent developments in the design of surfaces that prevent fouling by proteins, bacteria, and marine organisms. *Adv. Mater.* **2011**, *23*, 690-718.

34. Jeon, S. I.; Lee, J. H.; Andrade, J. D.; Degennes, P. G. Protein–surface interactions in the presence of polyethylene oxide. *J. Colloid Interface Sci.* **1991**, *142*, 149-158.
35. Jeon, S. I.; Andrade, J. D. Protein—surface interactions in the presence of polyethylene oxide: II. Effect of protein size. *J. Colloid Interface Sci.* **1991**, *142*, 159-166.
36. Harder, P.; Grunze, M.; Dahint, R.; Whitesides, G. M.; Laibinis, P. E. J. Molecular conformation in oligo(ethylene glycol)-terminated self-assembled monolayers on gold and silver surfaces determines their ability to resist protein adsorption. *Phys. Chem. B* **1998**, *102*, 426–436.
37. Sharpless, K. B.; Hartmuth, C.; Kolb, M.; Finn, G. Click chemistry: diverse chemical function from a few good reactions. *Angew. Chem. Int. Ed.* **2001**, *40*, 2004-2021.
38. Hoyle, C.E.; Bowman, C.N. Thiol-ene click chemistry. *Angew. Chem. Int. Ed.* **2010**, *49*, 1540-1573.
39. Lowe, A.B. Thiol-ene “click” reactions and recent applications in polymer and materials synthesis. *Polym. Chem.* **2010**, *1*, 17–36.
40. Hoyle, C. E.; Lee, T. Y.; Roper, T. Thiol–enes: chemistry of the past with promise for the future. *J. Polym. Sci. Part A* **2004**, *42*, 5301–5338.
41. Campos, L.M.; Meinel, I.; Guino, R.G.; Schierhorn, M.; Gupta, N.; Stucky, G.D.; Hawker, C.J. Highly versatile and robust materials for soft imprint lithography based on thiol-ene click chemistry. *Adv. Mat.* **2008**, *20*, 3728-3733.
42. Zhang, Z.; Feng, X.; Luo, Q.; Liu, B-F. Environmentally friendly surface modification of PDMS using PEG polymer brush. *Electrophoresis* **2009**, *30*, 3174-3180.
43. Sui, G.; Wang, J.; Lee, C-C.; Lu, W.; Lee, S. P.; Leyton, J. V.; Wu, A. M.; Tseng, H-R. Solution-phase surface modification in intact poly(dimethylsiloxane) microfluidic channels. *Anal. Chem.* **2006**, *78*, 5543-5551.
44. Cleland, W. W. Dithiothreitol, a new protective reagent for SH groups. *Biochemistry* **1964**, *3*, 480-482.

45. Wang, X.; Hu, W.; Ramasubramaniam, R.; Bernstein, G. H.; Snider, G.; Lieberman, M. Formation, characterization, and sub-50-nm patterning of organosilane monolayers with embedded disulfide bonds: an engineered self-assembled monolayer resist for electron-beam lithography. *Langmuir* **2003**, *19*, 9748-9758.
46. Young, T. An essay on the cohesion of fluids. *Philos. Trans. R. Soc. London* **1805**, *95*, 65-87.
47. Yuan, Y. and Lee, T.R. Bracco, G (Eds)., Holst, B. (Eds). Contact angle and wetting properties. *Surface science techniques* **2013**, Chapter 1, 3-34.
48. Tadmor, R. Line energy and the relation between advancing, receding, and young contact angles. *Langmuir* **2004**, *20*, 7659-7664.
49. Butt, H.J.; Cappella, B.; Kappl, M. Force measurements with the atomic force microscope: technique, interpretation and applications. *Surf. Sci. Rep.* **2005**, 591-152.
50. Gresse, N.A. AFM and combined optical techniques. *Mater. Today.* **2009**, *12*, 40-45.
51. "TappingMode Imaging Applications and Technology". Veeco, Inc. 2004.
52. Thundat, T.; Zheng, X. Y.; Chen, G. Y.; Warmack R. J. Role of relative humidity in atomic force microscopy imaging. *Surf. Sci.* **1993**, *294*, L939-L943.
53. RCSB Protein Data Bank. <http://www.rcsb.org/> (accessed April 2, 2015).
54. Sigma-Aldrich. <http://www.sigmaaldrich.com/> (accessed February 5, 2015).
55. Kragh-Hansen, U.; Chuang, V.T.G.; Otagiri, M. Practical aspects of the ligand-binding and enzymatic properties of human serum albumin. *Biol. Pharm. Bull.* **2002**, *25*, 695-704.
56. Lee, W. J.; Whitesides, G.M. Equilibrium constants for thiol-disulfide interchange reactions: A corrected coherent set. *J. Org. Chem.* **1993**, *58*, 642-647.

Appendix 1: PEGylation of PMMS substrates

Comparison of thickness, contact angle and AFM RMS values of SMS 042 and SMS 992 grafted with EG and OEG layers

	Contact Angle (θ_A^0 / θ_R^0)	Thickness of thiol layer (\AA)	Thickness of PEG layer (\AA)	RMS (\AA)
SMS 042	102±1/84±4	38±2	0	11±2
SMS042 + EG	103±2/75±0	34±1	-4±1	-
SMS 042 + OEG	102±2/66±2	35±1	-3±1	-
SMS 992	82±1/45±2	30±4	0	6±2
SMS 992+EG	52±1/34±2	31±1	1±1	5±2
SMS 992+OEG	46±2/31±2	54±3	24±3	10±2

Appendix 2: Calculation of amount of reducing agent in SMS 992 solution

Sample calculation for 1.5 wt % of DTT in SMS 992

Specific gravity of SMS 992 = 0.97 g/mL

15 mg DTT in 1 mL SMS 992 = $(0.015\text{g}/1\text{mL}) * (1\text{mL}/0.97\text{g}) * 100 = 1.5 \text{ wt } \%$

Appendix 3: Effect of reducing agents on SMS 992 layers

Changes in thickness, contact angles and average RMS values of the SMS 992 layers due to the addition of increasing amounts of DTB

	Contact angle ($\theta_A^\circ / \theta_R^\circ$)	Thickness (Å)	Average RMS (Å)
SMS 992	82±1/45±2	30±4	6±2
DTB-1.5 wt %	81±1/40±1	23±1	7±1
DTB-3.1 wt %	81±1/42±3	23±1	4±1
DTB-6.2 wt %	81±1/40±0	25±4	4±1
DTB-12.0 wt %	81±2/43±1	22±1	3±1

Changes in thickness, contact angles and average RMS values of the SMS 992 layers due to the addition of increasing amounts of DTT

	Contact angle ($\theta_A^\circ / \theta_R^\circ$)	Thickness (Å)	Average RMS (Å)
SMS 992	82±1/45±2	30±4	6±2
DTT-1.5 wt %	82±1/42±3	24±4	4±2
DTT-3.1 wt %	83±2/45±6	29±5	4±1
DTT-6.2 wt %	81±0/40±3	20±5	3±1
DTT-12.0 wt %	81±2/44±1	18±7	3±1

Appendix 4: PEGylation of SMS 992 reduced with 6.0 wt % of DTT

Comparisons among various substrates with and without the use of DTT as a reducing agent in the grafting of SMS 992.

	Contact angle ($\theta_A^\circ / \theta_R^\circ$)	Thickness of SMS 992 layer (\AA)	Average RMS (\AA)
SMS 992	82±1/45±2	30±4	6±2
SMS 992+EG	52±1/34±2	31±1	5±2
SMS 992+OEG	46±2/31±2	54±3	10±2
SMS 992 + DTT	81±1/40±0	25±4	4±1
SMS 992+DTT+EG	57±1/36±1	27±3	3±1
SMS 992 + DTT + OEG	45±2/31±0	44±4	8±4

Appendix 5: Protein resistance of PEGylated substrates

Changes in thickness, contact angle and RMS values of various substrates upon adsorption with PBS (control).

	Contact angle ($\theta_A^\circ / \theta_R^\circ$)	Thickness (\AA)	Average RMS (\AA)
SMS 992 + PBS	81 \pm 1/14 \pm 5	38 \pm 9	4 \pm 1
SMS 992+ EG + PBS	60 \pm 1/31 \pm 0	39 \pm 3	7 \pm 3
SMS 992 + OEG + PBS	44 \pm 1/29 \pm 0	45 \pm 6	6 \pm 1

Changes in thickness, contact angle and RMS values of various substrates upon adsorption with albumin.

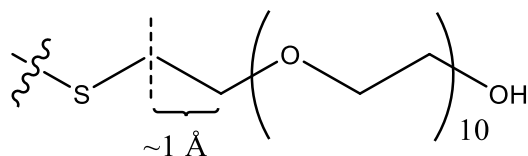
	Contact angle ($\theta_A^\circ / \theta_R^\circ$)	Thickness (\AA)	Average RMS (\AA)
SMS 992 + albumin	78 \pm 4/12 \pm 2	46 \pm 1	8 \pm 1
SMS 992+ EG + albumin	62 \pm 6/34 \pm 6	27 \pm 3	4 \pm 1
SMS 992 + OEG + albumin	53 \pm 1/28 \pm 1	40 \pm 2	7 \pm 1

Changes in thickness, contact angle and RMS values of various substrates upon adsorption with lysozyme.

	Contact angle ($\theta_A^\circ / \theta_R^\circ$)	Thickness (\AA)	Average RMS (\AA)
SMS 992 + lysozyme	71 \pm 6/11 \pm 2	60 \pm 1	13 \pm 2
SMS 992+ EG + lysozyme	57 \pm 1/28 \pm 1	45 \pm 1	65 \pm 15
SMS 992 + OEG + lysozyme	50 \pm 1/29 \pm 1	50 \pm 1	15 \pm 1

Thickness of protein layer

	SMS 992 (Å)	SMS + EG (Å)	SMS + OEG (Å)
PBS	18±6	8±2	-9±3
Albumin	26±5	-4±2	-14±3
Lysozyme	40±3	14±1	-4±2

Appendix 6: Calculation of approximate length of OEG chain

$$\text{Total number of bonds} = 1 + 1 + (3 \times 10) + 1 = 33$$

$$\text{Length of OEG chain (if shadow of the bonds is considered } \sim 1 \text{ \AA)} = 33 \times 1 \text{ \AA}$$

$$= 33 \text{ \AA}$$